THE JOURNAL OF BIOLOGICAL CHEMISTRY VOL. 291, NO. 7, pp. 3302–3318, February 12, 2016

Role of the C-terminal Extension of Formin 2 in Its Activation by Spire Protein and Processive Assembly of Actin Filaments*

Received for publication, July 24, 2015, and in revised form, December 4, 2015 Published, JBC Papers in Press, December 14, 2015, DOI 10.1074/jbc.M115.681379

Pierre Montaville[1], **Sonja Kühn**[1], **Christel Compper, and Marie-France Carlier**[2]

From the Cytoskeleton Dynamics and Motility, Institut de Biologie Intégrative de la Cellule, CNRS, 91198 Gif-sur-Yvette, France

Formin 2 (Fmn2), a member of the FMN family of formins, plays an important role in early development. This formin cooperates with profilin and Spire, a WASP homology domain 2 (WH2) repeat protein, to stimulate assembly of a dynamic cytoplasmic actin meshwork that facilitates translocation of the meiotic spindle in asymmetric division of mouse oocytes. The kinase-like non-catalytic domain (KIND) of Spire directly interacts with the C-terminal extension of the formin homology domain 2 (FH2) domain of Fmn2, called FSI. This direct interaction is required for the synergy between the two proteins in actin assembly. We have recently demonstrated how Spire, which caps barbed ends via its WH2 domains, activates Fmn2. Fmn2 by itself associates very poorly to filament barbed ends but is rapidly recruited to Spire-capped barbed ends via the KIND domain, and it subsequently displaces Spire from the barbed end to elicit rapid processive assembly from profilin·actin. Here, we address the mechanism by which Spire and Fmn2 compete at barbed ends and the role of FSI in orchestrating this competition as well as in the processivity of Fmn2. We have combined microcalorimetric, fluorescence, and hydrodynamic binding assays, as well as bulk solution and single filament measurements of actin assembly, to show that removal of FSI converts Fmn2 into a Capping Protein. This activity is mimicked by association of KIND to Fmn2. In addition, FSI binds actin at filament barbed ends as a weak capper and plays a role in displacing the WH2 domains of Spire from actin, thus allowing the association of actin-binding regions of FH2 to the barbed end.

Polarized assembly of actin filaments is pivotal in motile processes. It is precisely regulated by proteins that bind the barbed ends of actin filaments and either block or assist filament assembly using various mechanisms (1). Among these regulators, formins are acknowledged to nucleate and track filament barbed ends, mediating rapid processive elongation of filaments (2, 3). In contrast, WASP homology 2 (WH2)[3] repeat-containing proteins display versatile barbed end capping or tracking and filament severing activities (4). In early oogenesis of *Drosophila* as well as in mammalian meiosis, a formin (Fmn2/Cappuccino) and a WH2-repeat protein (Spire) synergize in an intriguing fashion to stimulate massive assembly of a dynamic cytoplasmic actin meshwork, required for completion of crucial steps in axis patterning or asymmetric division (5–12). This complexity adds to the known need of profilin for rapid processive assembly of all formins, including Cappuccino (9).

Like most formins, Fmn2 harbors conserved C-terminal formin homology 1 (FH1) and formin homology 2 (FH2) domains. The C-terminal FH1-FH2 domain of Fmn2 represents a constitutive active module in which the FH1 domain binds profilin and the FH2 domain to the barbed end of F-actin. The head-to-tail FH2 dimer of formins is thought, from structural data, to encircle the terminal and subterminal actin subunits that constitute the barbed end of the filament and to cycle between "closed" and "open" states during its processive walk (2, 13, 14). In contrast to the much better characterized group of Diaphanous-related formins, the Fmn formin family is not regulated by Rho GTPases. Additionally, the C-terminal auto-regulatory DAD region of Diaphanous formins is replaced by a short "tail," also called Formin-Spire-Interaction (FSI) peptide, because it binds the isolated N-terminal KIND domain of the Spire protein (15–17).

Spire is a modular actin-binding protein whose N-terminal constitutively active region (Nt-Spire) consists of an N-terminal KIND domain followed by four consecutive WH2 domains, which confer multifunctional actin assembly activities to Spire. All WH2 domains interact with the barbed face of actin that is exposed on G-actin and on the two terminal subunits of filament barbed ends (1, 4). Thus, Nt-Spire has several effects on actin assembly. It nucleates filaments from free G-actin (11), sequesters G-actin into a non-polymerizable complex, caps barbed ends with nanomolar affinity, and severs filaments (18). Barbed end capping prevents growth of filaments from profilin·actin and is likely the main function of Spire in cells where nucleation is abolished by profilin (18).

How Spire and Fmn2 synergize in stimulating actin assembly, while both proteins individually bind barbed ends with antagonistic effects on filament assembly, is an elusive issue. Biochemical approaches demonstrated that the FH1-FH2 module of Fmn2 by itself poorly nucleates filaments from profilin·actin and associates weakly and extremely slowly to free barbed ends but is rapidly recruited to Nt-Spire-bound barbed ends (BS) via the strong KIND-FSI interaction. Subsequent release of Spire from the ternary complex (BSF) sets up fast processive

* This work was supported by European Research Council Advanced Grant 249982 "Forcefulactin" and FP7 Program 241548 "MitoSys" (to M. F. C.). The authors declare that they have no conflicts of interest with the contents of this article.

[1] Both authors contributed equally to this work.

[2] To whom correspondence should be addressed. Tel.: 33-1-69823465; E-mail: marie-france.carlier@i2bc.paris-saclay.fr.

[3] The abbreviations used are: WH2, WASP homology domain 2; Fmn2, formin 2; FH1, formin homology domain 1; FH2, formin homology domain 2; FSI, formin Spire interaction; KIND, kinase-like non-catalytic domain; 1,5-I-AEDANS, *N*-iodoacetyl-*N*′-(5-sulfo-1-naphthyl)ethylenediamine; SA, spectrin-actin; PA, profilin·actin; ITC, isothermal titration calorimetry; Nt-Spire, N-terminal Spire; BS, Spire-bound barbed end; BF, Fmn2-bound barbed end; BSF, barbed end·Spire·Fmn2 complex.

elongation by Fmn2 (19). Thus, the Nt-Spire works as an actual activator of Fmn2. Filaments exposed to both proteins display alternate phases of arrested growth (BS state) and fast growth (BF state) via formation of a transient ternary BSF complex. This assembly profile was proposed to contribute to organizing a dynamic vesicle-filament network that fluidizes the oocyte cytoplasm and allows translocation of the spindle (19–21). Spire and Fmn2 stand as the second example of two proteins regulating filament assembly by binding together at the barbed end in a transient ternary complex. Other examples include the multiple WH2 domain protein VopF and Capping Protein (22) and more recently formin and Capping Protein (23, 24).

The interaction between the FSI tail of Fmn2 and the KIND domain of Spire is a prerequisite for the synergy between the two proteins. Recent mutagenesis studies of the Cappuccino tail indicated that this region, although different from other C-terminal regions of formins, binds G-actin and enhances actin nucleation as well as processivity in Cappuccino. These effects were recapitulated by replacing the original tail of Capuccino by the DAD domain of other formins (15).

Here, we address the role of the FSI region of Fmn2 in its activation of actin assembly by Spire and its processive cycle. We find that deletion of FSI from Fmn2 converts the formin into a Capping Protein and reduces the processive activity of Fmn2. Binding of the isolated KIND domain to Fmn2 recapitulates the effects of FSI deletion. In addition, FSI binds G-actin and weakly caps the barbed end of actin filaments in an ionic strength-dependent fashion. We analyze the binding of the isolated FSI and of the FH2 domain to the isolated KIND domain and to Nt-Spire. The presence of the non-actin-bound WH2 domains in Nt-Spire weakens the interaction of the KIND domain with FSI. The results are integrated into a model for activation of Fmn2 by Spire and for facilitation of Fmn2 processive assembly by FSI.

Experimental Procedures

Plasmid Constructs—The Fmn2, Fmn2ΔFSI, FH2, Nt-Spire (KIND-ABCD), and KIND constructs are identical to the ones described elsewhere (13). The Fmn2 construct is a chimera protein containing the FH1 domain of mDia1 (Ser-568–Pro-747, UniProt accession number NP_031884) followed by the FH2 domain of mouse formin 2 (Phe-1128–Thr-1578, NP_062318.2). The FH2ΔFSI (Gln-1134–Ser-1558) construct was subcloned from the Fmn2 cDNA sequence into the modified pGEX-6P1 expression vector using the restriction sites BamHI and XhoI. Triple glutamate to alanine mutations (E1546A/E1548A/ E1549A) were introduced in the Fmn2 and Fmn2ΔFSI constructs using the site-directed mutagenesis kit from Agilent Technologies (QuickChange II XL) and the following forward (5′-CGTGTGAAAGCAGCGGCTGCAGTTTGCCGCC-3′) and reverse (5′-GGCGGCAAACTGCAGCCGCTGCTTTCACACG-3′) primers. For construct borders and domain composition see Fig. 1*A*.

Protein Expression and Purification—Fmn2 and Spire (NP 001122098) protein constructs were expressed overnight at 16 °C in *Escherichia coli* Rosetta (DE3) strains (Novagen) in Luria-Bertani medium with 1 mM isopropyl 1-thio-β-D-galactopyranoside. Bacteria were harvested, pelleted, and resuspended in lysis buffer (20 mM Hepes, pH 7.5, 900 mM NaCl, 3 mM DTT, 0.1 mM EDTA, 15 mM imidazole, 5% sucrose, protease inhibitor mixture (CLAP), 5 μM benzamidine, 1 μM PMSF, DNase A, lysozyme, 1% Triton X-100) and sonicated on ice. Following ultracentrifugation, the cleared lysates were loaded on pre-equilibrated HisTrap crude FF columns (GE Healthcare) with binding buffer I (20 mM Hepes, pH 7.5, 900 mM NaCl, 3 mM DTT, 0.1 mM EDTA, 15 mM imidazole, pH 7.5, 5% sucrose) using an Akta prime chromatography system (GE Healthcare). The resin was washed with binding buffer I containing 4% elution buffer I (20 mM Hepes, pH 7.5, 900 mM NaCl, 3 mM DTT, 0.1 mM EDTA, 250 mM imidazole, pH 7.5, 5% sucrose) and proteins were eluted with a 60% elution buffer I gradient step. Salt concentration of the elution buffer was then decreased to 300 mM NaCl using a suitable volume of 50 mM Hepes, pH 7.5, buffer. The protein solution was then loaded on a StrepTrap HP column (GE Healthcare) pre-equilibrated with binding buffer II (50 mM Hepes, pH 7.5, 300 mM NaCl, 3 mM DTT, 1 mM EDTA, 5% sucrose). The resin was washed with binding buffer II, and bound proteins were eluted with binding buffer II supplemented with 4 mM desthiobiotin. After concentration of the elution fraction with a Vivaspin 10-kDa molecular mass cutoff, the protein solution was gel-filtered on a Superdex 200 16/60 (GE Healthcare) pre-equilibrated with GF buffer (20 mM Hepes, pH 7.5, 300 mM NaCl, 1 mM DTT, 1% sucrose). Fractions containing pure proteins were pooled, concentrated, flash-frozen, and stored at −80 °C. For the FH2 and KIND construct, an additional N-terminal histidine-thioredoxin overnight cleavage step was performed before the StrepTrap affinity column using PreScission protease (5 units/mg fusion protein) at 4 °C. For the Nt-Spire construct, the StrepTrap affinity column step was replaced by an overnight GST tag cleavage step before size exclusion chromatography using PreScission protease (5 units/mg of fusion protein) at 4 °C.

G-actin was purified from rabbit muscle, pyrenyl-, or AEDANS labeled on cysteine 374 as described (18) or Alexa-488 labeled on surface lysines (19). Thymosin β4, profilin, and spectrin-actin seeds were prepared as described (13).

The FSI peptide comprising the last 30 residues of the mouse Fmn2 sequence (Glu-1549–Thr-1578) was chemically synthetized (Proteogenix). The peptide was dissolved in double distilled H_2O, loaded on a pre-equilibrated PD-10 desalting column, and eluted in FSI buffer (20 mM Tris/HCl, pH 7.8, 1 mM DTT, 150 mM NaCl). The FSI extinction coefficient was calculated (25) ($\epsilon_{205\,nm}$ = 91,960 M^{-1} cm^{-1}), and concentrations were measured at 205 nm.

Isothermal Titration Calorimetry—Interactions of mouse formin Fmn2 constructs or peptides with human Spire-1 proteins were performed by isothermal titration calorimetry (ITC) using a MicroCal iTC200 microcalorimeter (GE Healthcare). Measurements were carried out in 20 mM Tris/HCl, pH 7.5, 150 mM NaCl, and 0.8 mM dithioerythritol at 298 K. FSI peptide at 350 μM or FH2 (FH2-FSI of Fmn2, amino acids Phe-1128–Thr-1578) at a concentration of 500 μM were stepwise injected from the syringe to 35 or 50 μM Kind (Spire1, amino acids Gly-35–Ser-257) or Nt-Spire (Spire1, amino acids M1-S443) placed in the measurement cell. The change in heating power was observed over the reaction time until equilibrium was reached.

Data were analyzed using the software provided by the manufacturer.

Size Exclusion Chromatography—Analytical gel filtration experiments of several Fmn2 and Spire constructs in the presence or absence of G-actin were performed using an Akta prime chromatography system (GE Healthcare) equipped with a Superdex S200 (10/300 GL) column (GE Healthcare). Typically, 10 μM of each protein were loaded onto the column that was pre-equilibrated in GF buffer II (20 mM Tris/HCl, pH 7.8, 50 or 150 mM NaCl, 1 mM DTT) prior to injection of the protein samples. 0.1 μM G-actin was added to the GF buffer II for gel filtration samples of potential G-actin-containing complexes. Gel filtrations were run at room temperature at a flow rate of 0.5 ml per min and were repeated several times. The optical density was monitored at a wavelength of 280 nm over the time course of the experiment. The column was calibrated using standard globular proteins (Amersham Biosciences) spanning 6.5 kDa (*Rh* = 13.50 Å) to 669 kDa (*Rh* = 85.0 Å). The hydrodynamic radius (*Rh*) calibration was derived from the plot of $(-\log K_{AV})1/2$ *versus Rh* with $K_{av} = (V_e - V_o)/(V_t - V_o)$, where V_e is the elution volume for the protein; V_o is the column void volume (7.3 ml), and V_t is the total bed volume (20.3 ml).

Fluorescence Measurements of FSI-Actin Interaction—Proteins were labeled on cysteines using 1,5-I-AEDANS. Fluorescence titration measurements were carried out using either AEDANS-actin (λex = 347 nm, λem = 460 nm) or AEDANS-FSI (λex = 354 nm, λem = 498 nm) in G buffer (5 mM Tris/HCl, pH 7.8, 0.2 mM ATP, 0.1 mM $CaCl_2$, 1 mM DTT), including salt as indicated. To minimize unspecific binding of FSI or inactivation during the experiments, all samples were prepared individually for each concentration step. Experiments were carried out at 20 °C in a Safas Xenius model FLX spectrofluorimeter (Safas, Monaco) equipped with a device for automatic anisotropy measurements, or in a FluoroMax-4 spectrofluorometer (Horiba Scientific). Salt concentrations were strictly kept constant in all samples of the particular titration runs.

Kinetic and Steady-state Measurements of Actin Assembly—Spontaneous actin assembly, seeded barbed end growth, and dilution-induced depolymerization assays were performed using the change in fluorescence of 5% pyrenyl-labeled actin (λex = 366 nm, λem = 407 nm) as described (19). Assays were performed in G buffer (5 mM Tris/Cl, pH 7.8, 0.2 mM ATP, 0.1 mM $CaCl_2$, 1 mM DTT) supplemented with 1 mM $MgCl_2$, 0.2 mM EGTA, and either KCl or NaCl at 0, 50, or 100 mM as indicated (F buffer). Prior to each experiment, a stock solution of 10 μM Ca^{2+}ATP-G-actin was converted into Mg^{2+} ATP-G-actin by addition of 20 μM $MgCl_2$ and 0.2 mM EGTA and kept on ice. Profilin was added to this stock solution at final concentrations as indicated. All experiments were carried out at 20 °C in a Safas Xenius FLX spectrofluorimeter using a multiple sample device.

Steady-state measurements of F-actin (2% pyrenyl-labeled) assembly were conducted after overnight incubation at 4 °C in the dark of samples containing 2.5 μM F-actin and proteins (profilin, FSI, or different Fmn2 constructs) as indicated. Samples were equilibrated for 1 h at 20 °C prior to readout. Dilution-induced depolymerization of actin filaments was performed by a 16× dilution of preformed, 5 μM F-actin (50% pyrenyl-labeled, non-capped, or gelsolin-capped with a 1:250 gelsolin:actin ratio) in F buffer with FSI amounts as indicated. The initial rate of the decrease in pyrenyl-actin fluorescence was measured and normalized regarding to the initial depolymerization rate in control samples. Light scattering measurements were performed at 310 nm in the spectrofluorimeter.

TIRF Microscopy of Single Filaments—The bundling effect of FSI was investigated with standard TIRF microscopy assays using a flow chamber assembled by placing two parallel strips of parafilm onto a cleaned glass slide, surmounted with a PLL-PEG passivated coverslip. Chambers were washed with G buffer, 5% BSA, and F buffer supplemented with 50 mM KCl and 0.2% methylcellulose (Sigma catalog no. M-0262). Assays were performed in this modified F buffer with 1 μM Alexa-488-labeled G-actin, 4 μM profilin, 0.3 nM spectrin-actin seeds, and FSI at indicated concentrations.

Microfluidics-assisted TIRF microscopy assays were performed using polydimethyl-sulfoxane flow cells with three inlets. Microfluidic chambers were prepared as follows. For one chamber, a coverslip was successively sonicated in double distilled H_2O, ethanol, and acetone for 10 min each, then in 1 M KOH (20 min), in double distilled H_2O (10 min), and finally in ethanol (10 min). After air drying, coverslips were exposed to a plasma discharge for 2 min (Elmo Glow discharge system, Cordouan Technologies) and assembled with a 3 inlets-1 outlet polydimethyl-sulfoxane chamber (26). The microchamber was filled with 50 μl of a solution of 5 mM PEG silane (M_r 5000, Laysan Bio) in DMSO for 20 min and then rinsed with G buffer supplemented with 0.1% bovine serum albumin for 30 min and with Fluo F buffer (5 mM Tris/HCl, pH 7.8, 0.2 mM ATP, 20 mM DTT, 1 mM $MgCl_2$, 1 mM 1,4-diazabicyclo[2.2.2]octane, 0.01 % (w/vol) NaN_3 supplemented with 50 or 100 mM NaCl). The microchamber was then taped on the microscope stage and connected to the microfluidic setup (MFCS and Flowell from Fluigent). Experiments were conducted as follows: spectrin-actin (SA) seeds were first adsorbed on the glass surface by flowing in 5 pM SA in fluo F buffer for 5 min at 7 μl/min. Filament barbed end growth was initiated by flowing in profilin and G-actin (5% labeled with Alexa-488 succinimidyl ester) in fluo F buffer for at least 200 s at 4 μl/min, and the same condition was supplemented with the chosen amount of the protein of interest.

TIRF observations were acquired using a cascade II EMCCD camera (Photometrics) on an Olympus IX71 inverted microscope, with a ×60 TIRF objective (512 × 512 pixel field of view, 1 pixel being 267 nm in side length and corresponding to about 99 actin subunits), and a 473-nm laser (Cobolt). The experiments were controlled using the Metamorph software. Typical movies were recorded for 181 frames with a frame interval of 10 s and were further analyzed by ImageJ to obtain kymographs. A change in growth rate was associated with the binding of regulators to the barbed ends. The fraction of filament population that changes growth rate *versus* time thus represents the time course of association with barbed ends. Kinetics were displayed as cumulative distribution functions of filaments in a given state of growth *versus* time and fit with single exponential curves using Igor Pro (WaveMetrics). The association rate was calculated as the observed monoexponential divided by the

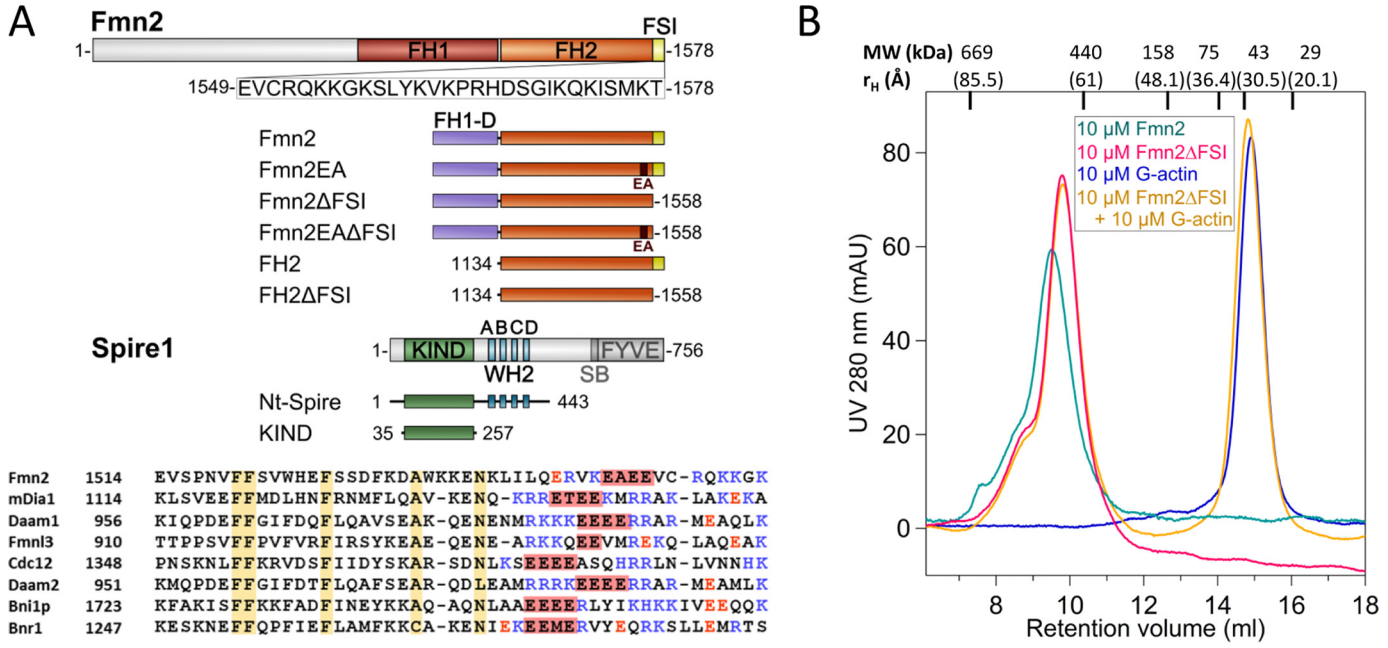

FIGURE 1. **Structural organization and hydrodynamic parameters of Fmn2 and Spire protein constructs used in this study.** *A,* domain organization of C-terminal Fmn2 and N-terminal Spire constructs and sequence alignment of the C-terminal αT-helix of various FH2 domains, emphasizing the existence of a conserved acidic patch (*boxed* in *red*) in a basic environment. Identical residues in αT-helix are boxed in *yellow*; basic residues are *blue*; acidic residues are *red*. In the Fmn2EA and Fmn2EAΔFSI constructs, the ^{1546}EAEE^{1549} amino acid sequence of Fmn2 is mutated to AAAA. FH1-D (*purple*) represents the FH1 domain of mDia1, which replaces the FH1 domain of formin 2 in the chimeric Fmn2 construct. The accession numbers for protein sequences displayed in the alignment are as follows: NP_062318.2 (Fmn2), O08808 (mDia1), AAH38428.1 (Daam1), Q6ZPF4 (Fmnl3), CAA92232 (Cdc12), Q86T65 (Daam2), P41832 (Bni1p), and AJR53591 (Bnr1). *B,* Fmn2ΔFSI is dimeric. Size exclusion chromatography of Fmn2ΔFSI in comparison with Fmn2. Removal of FSI does not greatly affect the Stokes radius of Fmn2, implying that Fmn2ΔFSI remains dimeric. Fmn2ΔFSI, like Fmn2, does not bind G-actin.

concentration of regulator. The dissociation rate constant was the best fit monoexponential. Elongation rates were calculated from the slope in the fast processive elongation mode and converted into subunits/s using 370 subunits/μm of filament length and 262 nm/pixel.

Results

Removal of the FSI from FH1-FH2 of Fmn2 Facilitates Its Association to Filament Barbed Ends and Converts the Formin into a Weak Barbed End Capping Protein—To understand the regulatory activity of the C-terminal FSI region of Fmn2 in actin assembly, we used the construct $FH1_D$-FH2, which includes the FH1 domain of mDia1 fused to the FH2 domain of Fmn2. We previously showed that this construct recapitulates all properties of FH1-FH2 of Fmn2 (19) and has the advantage of being produced in larger amounts suitable for biochemical experimentation. The $FH1_D$-FH2 will be called Fmn2 for simplicity below. The construct lacking the 29 C-terminal residues of FH2, called Fmn2ΔFSI, was similarly expressed and purified using the same procedures (Fig. 1*A*) (19). This construct ends with the C-terminal elongated αT-helix of the FH2 domain. Based on structure-based sequence alignments with known FH2 domain structures, the structural elements of Fmn2 that determine its dimeric nature remain conserved in the Fmn2ΔFSI context. Size exclusion chromatography experiments confirmed that Fmn2ΔFSI elutes as a dimer (Fig. 1*B*), as it has been also shown for C-terminally truncated constructs of Capu (16). The smaller construct FH2ΔFSI, which lacks the FH1 domain, was also expressed and purified (Fig. 1*A*).

The effects of the Fmn2 FH2 domain in the presence or absence of the FSI tail on actin assembly were compared. Removal of FSI in the Fmn2ΔFSI construct practically abolished the already low nucleation activity of Fmn2 in the presence of profilin·actin (data not shown). Similar loss of nucleation, however, in the absence of profilin, was reported for the C-terminally truncated Cappuccino formin (15). How removal of FSI affected the association of Fmn2 to barbed ends and processive activity was examined using first a seeded barbed end growth assay. Fig. 2*A* recapitulates previous results obtained with Fmn2 and Spire (19) and compares them with new data with Fmn2ΔFSI and FH2ΔFSI. Although Fmn2 did not detectably affect seeded barbed end growth in similar assays, due to its very weak association to barbed ends, Fmn2ΔFSI as well as FH2ΔFSI at nanomolar amounts strikingly caused instant inhibition of barbed end growth from profilin·actin (Fig. 2*A*). Nt-Spire by itself capped barbed ends and prevented growth from profilin·actin. Barbed end elongation was restored by addition of Fmn2 to Nt-Spire-capped barbed ends, but it was not restored by addition of Fmn2ΔFSI. Shielding of the FSI in Fmn2 by interaction with the isolated KIND domain led to the same inhibitory effect on barbed end assembly as Fmn2ΔFSI and FH2ΔFSI (Fig. 2*A*). KIND did not affect the capping activity of Fmn2ΔFSI. Additionally, the concentration-dependent blockage of barbed end growth by FH2ΔFSI and Fmn2ΔFSI was affected by ionic strength (Fig. 2, *B–D*). At 50 mM NaCl, both constructs behaved as barbed end capping proteins that totally inhibited barbed end growth with a K_d of 6 ± 2 nM (Fmn2ΔFSI) and 47 ± 2 nM (FH2ΔFSI), respectively (Fig. 2*C*). At 100 mM NaCl, the interaction with barbed ends was 1 order of magnitude weaker (K_d = 40 ± 5 nM for Fmn2ΔFSI and K_d = 324 ± 29 nM for FH2ΔFSI) and conspicuously only 80%

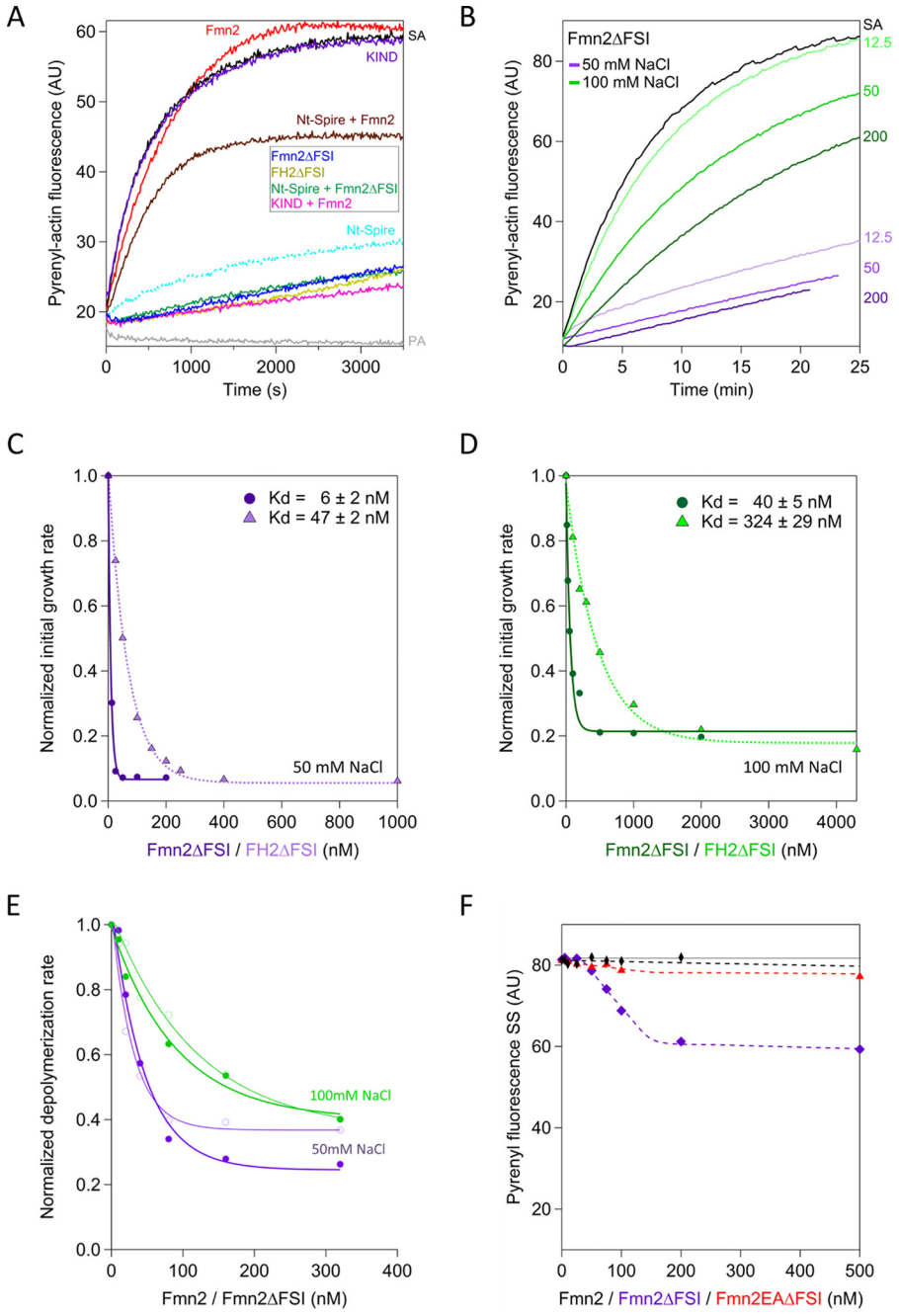

FIGURE 2. **Removal of FSI converts Fmn2 and its FH2 domain into an ionic strength sensitive barbed end capping protein.** *A,* removal of FSI inhibits the synergy between Fmn2 and Nt-Spire by preventing FSI-KIND interaction. Seeded barbed end growth of actin filaments in the presence of 0.42 nM SA seeds, 2.5 μM actin (5% pyrenyl-labeled), 6.5 μM profilin, 50 mM NaCl, and indicated proteins as shown as follows: no addition (*black*); 50 nM Fmn2 (*red*); 100 nM Fmn2ΔFSI (*blue*); 500 nM FH2ΔFSI (*ocher*); 1.3 μM KIND (*purple*); 1.3 μM KIND + 100 nM Fmn2 (*magenta*); 50 nM Nt-Spire (*light blue*); 50 nM Nt-Spire + 50 nM Fmn2 (*brown*); and 50 nM Nt-Spire + 100 nM Fmn2ΔFSI (*green*). The control curve for PA alone without spectrin-actin seeds is depicted in *light gray*. *B,* Fmn2ΔFSI blocks barbed end growth in an ionic strength sensitive fashion. Time courses of barbed end growth at 50 mM NaCl (*purple*) or 100 mM NaCl (*green*) were measured in the presence of 0.3 nM spectrin-actin seeds, 2.5 μM G-actin (5% pyrenyl-labeled), 6.5 μM profilin, and Fmn2ΔFSI concentrations as indicated in nanomolars. The curve for seeded barbed end growth without additional proteins is shown in *black* (*SA*). *C,* Fmn2ΔFSI and FH2ΔFSI block barbed end growth at 50 mM NaCl. The initial rate of seeded barbed end growth was measured in the presence of 0.3 nM spectrin-actin seeds, 2.5 μM G-actin (5% pyrenyl-labeled), 6.5 μM profilin, and indicated concentrations of Fmn2ΔFSI (*dark purple, circle*) or FH2ΔFSI (*light purple, triangle*). Rate values are normalized taking the growth rate without addition as the reference. Selected curves of pyrenyl-actin fluorescence over time of Fmn2ΔFSI are depicted in *B*. *D,* same as *C* except for 100 mM NaCl with Fmn2ΔFSI (*dark green, circle*) or FH2ΔFSI (*light green, triangle*). *E,* Fmn2ΔFSI (*closed symbols*) and Fmn2 (*open symbols*) identically block barbed end disassembly. Dilution-induced depolymerization of F-actin (final: 50 nM actin, 1% pyrenyl-labeled) was monitored in the presence of the indicated proteins at 50 mM (*purple*) or 100 mM (*green*) NaCl. *F,* evidence for weak barbed end capping activity of Fmn2ΔFSI at steady state. Actin (2.7 μM, 5% pyrenyl-labeled) was assembled in the presence of 7.5 μM profilin, 50 mM NaCl, and indicated amounts of Fmn2 (*black*), Fmn2ΔFSI (*purple*), or Fmn2EAΔFSI (*red*). Pyrene fluorescence was monitored after overnight incubation. *AU*, arbitrary units.

inhibition of barbed end growth was measured at saturating concentrations of FH2ΔFSI or of Fmn2ΔFSI (Fig. 2*D*). In dilution-induced depolymerization assays, Fmn2 and Fmn2ΔFSI similarly inhibited barbed end disassembly, again consistent with capping of barbed ends (Fig. 2*E*). Capping was more effective at 50 mM than at 100 mM NaCl. Remarkably, in the same

dilution-induced depolymerization assay, Fmn2 as well as FH2 have been shown to identically inhibit barbed end disassembly by capping barbed ends with similar affinities (supplemental Fig. 6 in Ref. 19). Thus, importantly, Fmn2 and Fmn2ΔFSI differ in their binding to barbed ends and their effects on net barbed end growth in the presence of G-actin, but identically cap barbed ends in a regime of disassembly. Finally, the capping of barbed ends by Fmn2ΔFSI was demonstrated in steady-state measurements of F-actin (Fig. 2*F*). F-actin disassembly into profilin·actin was observed, indicating barbed ends are capped upon addition of Fmn2ΔFSI but not upon addition of Fmn2.

In conclusion, removal of the FSI greatly facilitates association of Fmn2 to growing barbed ends, but it does not appear to stimulate assembly; rather it causes inhibition of barbed end growth. The behavior of all filaments is averaged in bulk solution measurements. As a result, at 100 mM NaCl we cannot conclude whether Fmn2ΔFSI slows the growth of all filaments or whether the measured slow average growth reached at saturation reflects the existence of a heterogeneous population of filaments, some being capped and others not.

To obtain the kinetic parameters for Fmn2ΔFSI association to and dissociation from filament barbed ends, to elucidate the nature of reactions that underlie the incomplete inhibition of growth by saturating amounts of Fmn2ΔFSI at physiological ionic strength, and to understand how FSI removal affects the processive cycle of Fmn2, single filament kinetics were performed. Microfluidics-assisted microscopy (26, 27) is the most appropriate method to analyze the function of actin regulatory proteins, in particular barbed end regulators, at the scale of individual filaments. Barbed end growth from profilin·actin (PA) was monitored on filaments that were initiated and anchored at their pointed ends by immobilized spectrin-actin seeds (see under "Experimental Procedures"). In the presence of 50 mM NaCl, addition of Fmn2ΔFSI to PA in the flowing solution caused arrest of filament growth. Representative kymographs are shown in Fig. 3*A*. The rate constant for association of Fmn2ΔFSI to growing barbed ends was derived from the time dependence of the fraction of filaments that stopped growing (Fig. 3*B*). A value of 2.72 μM^{-1} s^{-1} was found (Table 1). Thus, Fmn2ΔFSI associates 300-fold faster to barbed ends than the unmodified Fmn2, but in contrast to Fmn2, it binds in a capping closed conformation. Upon removal of Fmn2ΔFSI from the flowing solution, capped filaments resumed slow growth, characteristic of the association of profilin·actin to free barbed ends, indicating that Fmn2ΔFSI had dissociated from the barbed end. A value of 0.004 s^{-1} for the dissociation rate constant of Fmn2ΔFSI from barbed ends (*versus* 0.0037 s^{-1} for Fmn2) was derived from the time dependence of the fraction of filaments that resumed slow growth (Fig. 3*B*). Thus, Fmn2ΔFSI caps barbed ends with a K_d of 1.5 nM. Notably, in contrast with the association rate, the dissociation rate of Fmn2 from barbed ends is not affected by removal of FSI.

In the presence of 100 mM NaCl, two types of events were recorded upon continuous exposure of growing barbed ends to Fmn2ΔFSI (Fig. 3, *C* and *D*). A majority of short lived capping events characterized by alternating periods of pauses and resumed growth of 50–200 s each led to a global 50% slowing down of filament growth (Fig. 3*C*). The growing and pausing periods were too short to provide a realistic estimate of the rate constants for Fmn2ΔFSI association to and dissociation from the barbed ends. Very few rapid processive assembly events were recorded, corresponding to very slow association of Fmn2ΔFSI to barbed ends (k_{on} = 0.00125 μM^{-1} s^{-1}; Fig. 3*D*). Dissociation of Fmn2ΔFSI from processively assembling filaments occurred with a rate constant of 0.0036 s^{-1}. The rate of processive assembly (41 subunits/s) is almost identical to the one recorded for Fmn2 (53 subunits/s (19)).

In summary, the FSI appears to play a role in the transition of open to closed states of Fmn2. The effect of FSI removal leading to a capping activity is weaker at high ionic strength, because rare events of slow association of Fmn2ΔFSI to barbed ends leading to processive growth, as observed for Fmn2, can be detected, and the rate of processive assembly is not dependent on FSI. All rate and equilibrium parameters for Fmn2ΔFSI at barbed ends are summarized in Table 1.

We conclude that the presence of the FSI in Fmn2 hinders the interface of Fmn2 with the barbed end in a regime of growth and is somehow responsible for the very slow association rate of Fmn2 to barbed ends (19). The sensitivity of the hindrance/capping effect to ionic strength suggests that electrostatic interactions of FSI within the F-actin·FH2 complex at barbed ends are involved in its regulation of processivity of Fmn2.

Binding of the KIND Domain to Fmn2 Recapitulates the Effect of FSI Removal from Fmn2—The FSI targets the KIND domain of Spire (16, 17, 28, 29) by making mainly electrostatic contacts between a basic stretch of FSI and an exposed acidic patch of KIND. We reported that KIND inhibits Fmn2-stimulated spontaneous actin filament assembly from PA (19), but this mechanism was not addressed.

Compared effects of Fmn2 ± KIND, Fmn2 ± Nt-Spire, and Fmn2ΔFSI ± Nt-Spire on barbed end growth are shown in Fig. 2*A*. The data confirm and extend previous results (19). To understand how KIND inhibits Fmn2, seeded barbed end growth assays were performed at 50 and 100 mM NaCl as described for Fmn2ΔFSI. Association of KIND to Fmn2 converted Fmn2 into a barbed end capping protein (Fig. 4*A*). The affinity of the Fmn2·KIND complex for barbed ends was higher at 50 mM NaCl (K_d = 2 ± 0.5 nM) than at 100 mM NaCl (K_d = 12 ± 2 nM).

In contrast, in analysis of single filaments at 100 mM NaCl, only capping of barbed ends was observed. No processive event was detected with KIND-Fmn2. The on-rate constant of Fmn2·KIND to barbed ends was derived from the time course of filament capping following addition of Fmn2·KIND in the flow (Fig. 4, *B* and *C*). The off-rate constant was derived from the dwell time of Fmn2·KIND in the capped state. Rate constants for association and dissociation of Fmn2·KIND complex at barbed ends are summarized in Table 1.

In conclusion, binding of KIND to Fmn2 is in part functionally equivalent to removal of FSI from Fmn2 and leads to a release of FSI-mediated hindrance of the actin-binding modules present in the FH2 domain. The barbed ends become capped by Fmn2·KIND, and the maintenance of KIND binding to FSI prevents the onset of processive assembly by Fmn2. This result brings some light into the mechanism of activation of Fmn2 by Spire. The first step in formation of the BSF complex is

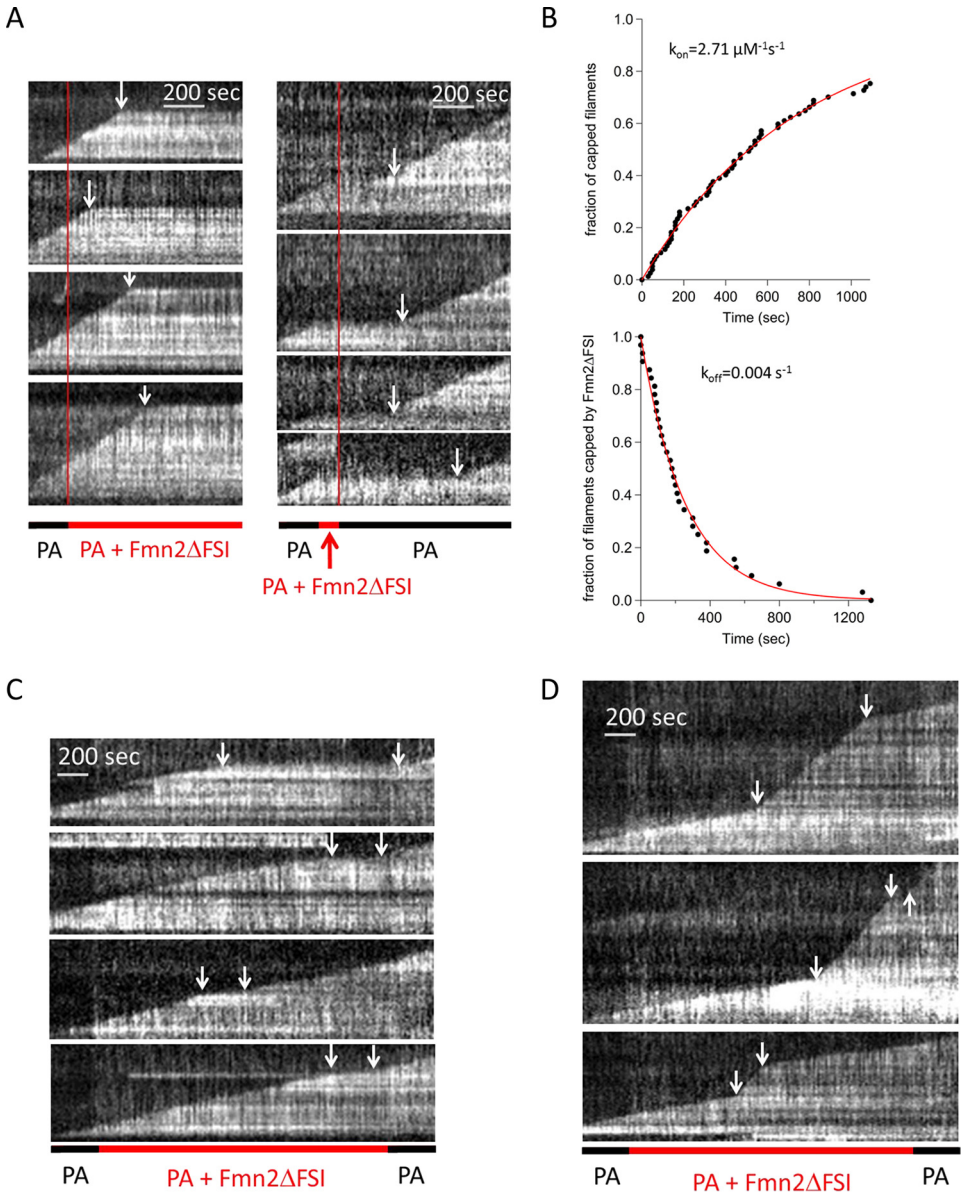

FIGURE 3. **Single filament analysis of the interaction of Fmn2ΔFSI with filament barbed ends using microfluidics-assisted TIRF microscopy.** *A*, 50 mM NaCl. Filaments grew from immobilized spectrin-actin seeds and were exposed to flowing solutions of various compositions as indicated. Conditions are as follows: 1 μM actin, 4 μM profilin, ± Fmn2ΔFSI. *Left panel,* representative kymographs of filament capping by association of 0.5 nM Fmn2ΔFSI to growing barbed ends. *Right panel,* kymographs illustrating the dissociation of Fmn2ΔFSI from barbed ends. Growing barbed ends were capped after exposure of 40 nM Fmn2ΔFSI for 30 s. Removal of Fmn2ΔFSI from the flow led to resumed growth of barbed ends from PA. *B*, analysis of data shown in *A*. *Upper panel,* fraction of capped filaments as a function of time. Data are fitted to a monoexponential process of rate constant k_{obs}. The rate constant for association of Fmn2ΔFSI to barbed end was derived as $k_{on} = k_{obs}/[Fmn2\Delta FSI]$. *Lower panel,* fraction of filaments remaining capped by Fmn2ΔFSI upon removal of Fmn2ΔFSI ($n = 77$ filaments). The dissociation rate constant of Fmn2ΔFSI from barbed ends was derived from the monoexponential dependence ($n = 32$ filaments). *C*, 100 mM NaCl. Kymographs of alternating Fmn2ΔFSI-capped and free states of filament barbed ends continuously exposed to PA (0.5 μM actin, 2 μM profilin) and 7 μM Fmn2ΔFSI are shown. *D*, kymographs of rare Fmn2ΔFSI-mediated, processive events recorded under the same conditions as in *C*.

TABLE 1

Kinetic parameters for interaction of Fmn2, Fmn2ΔFSI, Fmn2EA, and Fmn2EAΔFSI with barbed ends at 50 and 100 mM NaCl

	Fmn2	Fmn2ΔFSI		Fmn2/KIND	Fmn2EA	Fmn2EAΔFSI
NaCl (mM)	100	50	100	100	50	50
k_{on} (μM^{-1} s^{-1})	0.0074 ± 0.0005[a]	2.72 ± 0.035[b]	0.00125 ± 0.0001[a,c]	0.135 ± 0.0033[b]	0.004 ± 0.0004[a]	0.06 ± 0.0013[b]
k_{off} (s^{-1})	0.0037 ± 0.0002[a]	0.004 ± 0.0002[a]	0.0036 ± 0.0002[a,c]	0.002 ± 0.0005[b]	0.003 ± 0.0005[a]	0.0035 ± 0.0011[b]
Assembly rate (subunit s^{-1})	53 ± 6.2	ND[d]	41 ± 5.1	ND	51.6 ± 6.3	ND
Capping	No	Yes	Yes	Yes	No	Yes

[a] Rate constant refers to association leading to processive assembly (k_{on}) or dissociation leading to resumed free barbed end growth (k_{off}).
[b] Rate constant refers to association leading to capping (arrest of growth, k_{on}) or dissociation leading to resumed free barbed end growth (k_{off}).
[c] Rate constant refers to rare events of onset or arrest of processive assembly. Rapid equilibrium capping is the main event (see text).
[d] ND is not determined.

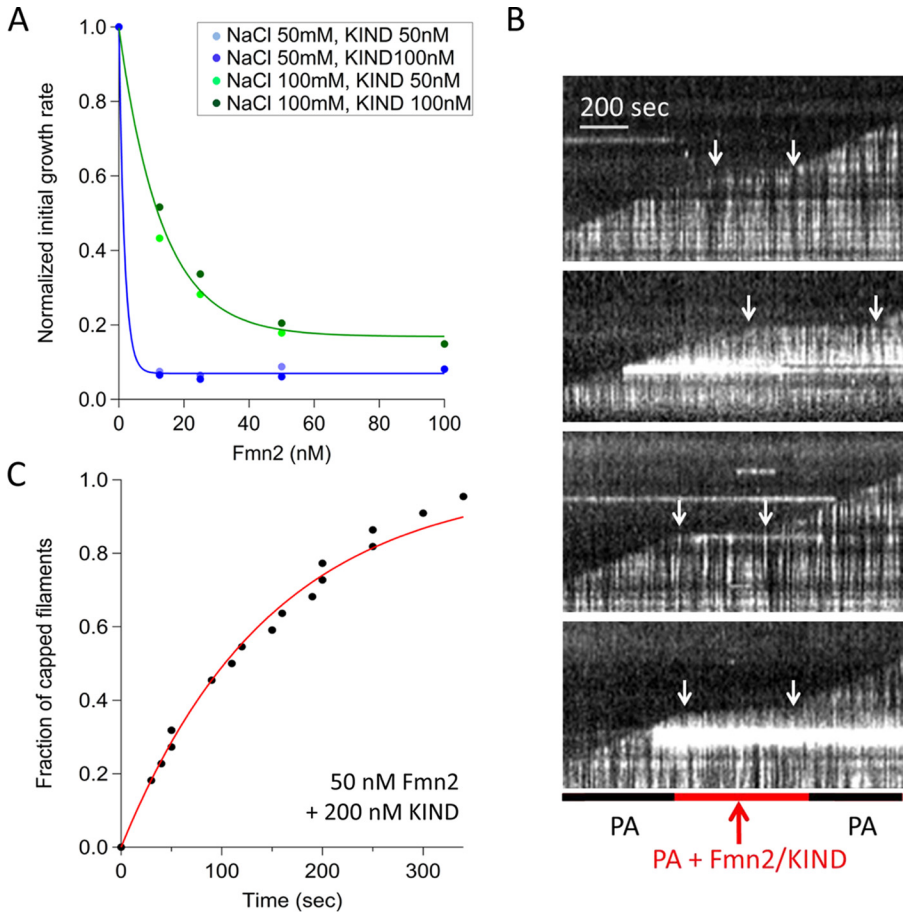

FIGURE 4. **Complex of Fmn2 with KIND caps barbed ends like Fmn2ΔFSI.** *A,* ionic strength sensitive barbed end capping by Fmn2·KIND. The rate of seeded barbed end growth was measured as in Fig. 2, *B–D,* in the presence of 50 nM (*light color*) or 100 nM KIND (*dark color*), of 50 mM NaCl (*blue*) or 100 mM NaCl (*green*), and of increasing amounts of Fmn2 as indicated. Values of the binding constants of Fmn2·KIND to barbed ends were 2 ± 0.5 nM at 50 mM NaCl and 12 ± 2 nM at 100 mM NaCl. *B,* single filament measurements of the kinetics of binding of Fmn2·KIND to barbed ends; representative kymographs of filament barbed end capping by Fmn2·KIND complex are shown. Flow contained 1 μM actin, 4 μM profilin, 200 nM KIND, 200 nM Fmn2, 100 mM NaCl. Note that dissociation of KIND-Fmn2 leading to resumed growth from PA sometimes occurs before removal of KIND and Fmn2 from the flow. *C,* kinetic analysis of Fmn2·KIND complex association to barbed ends at 100 mM NaCl. KIND and Fmn2 concentrations were 200 and 50 nM, respectively.

most likely the association of the FSI of Fmn2 to the KIND domain of barbed end-bound Nt-Spire (BS). At this point, at least one WH2 domain of Nt-Spire is bound to the barbed face of actin at barbed ends, preventing binding of FH2 in the capping conformation that is easily achieved with Fmn2·KIND. The WH2-binding site on actin actually overlaps with the FH2-binding site (1, 2, 13). How then is WH2 displaced from the barbed end by FH2 and how is the FSI-KIND contact subsequently disrupted, allowing the observed full dissociation of Nt-Spire from the barbed end (19)? What is the actin-binding mode of FSI in the Fmn2·F-actin complex at barbed ends and how is capping triggered rather than processive walk?

To answer these puzzling issues, we analyzed how the binding of FSI, either in isolation or within the FH2 domain context, to the KIND domain is affected by the WH2 domains of Nt-Spire, and we investigated whether FSI putatively interacts with actin at barbed ends.

Interaction of FSI and of FH2 with the Isolated KIND Domain and Nt-Spire—The binding of FSI to the isolated KIND domain and to Nt-Spire comprising KIND and all four WH2 domains (Fig. 1*A*) was explored in isothermal calorimetric studies (ITC) at 150 mM NaCl to be comparable with the previous Spire-Fmn2 studies (Fig. 5*A*). The thermodynamic parameters of these interactions are summarized in Table 2. Isolated FSI and the FH2 construct (consisting of the full FH2 domain and the adjacent FSI motif) displayed identical affinities for the KIND domain, which demonstrates that the KIND-binding site is fully exposed in FH2. In contrast, the affinity of FSI (or FH2) for the KIND domain decreased by 1 order of magnitude when the C-terminally adjacent WH2 domains were present in the Nt-Spire construct (Table 2 and Fig. 5*A*). Consistent with these findings, a tight complex of FH2 and KIND was eluted from a size exclusion column, but no complex of FH2ΔFSI and KIND was detected in gel filtration experiments (Fig. 5*B*). In contrast with KIND, Nt-Spire did not form a complex with FH2 (Fig. 5*C*). However, when actin together with Nt-Spire and FH2 was loaded, then a ternary complex FH2·Nt-Spire·actin was eluted (Fig. 5*C*). In conclusion, gel filtration experiments confirm that the affinity of FH2 for KIND is decreased by the presence of unliganded WH2 domains in Nt-Spire. The results further suggest that binding of actin (either G-actin or terminal F-actin at barbed ends) to WH2 of Nt-Spire neutralizes the inhibitory effect and restores a high affinity of FH2 for Nt-Spire. The fact that Fmn2 readily associates to Spire-bound barbed ends via the

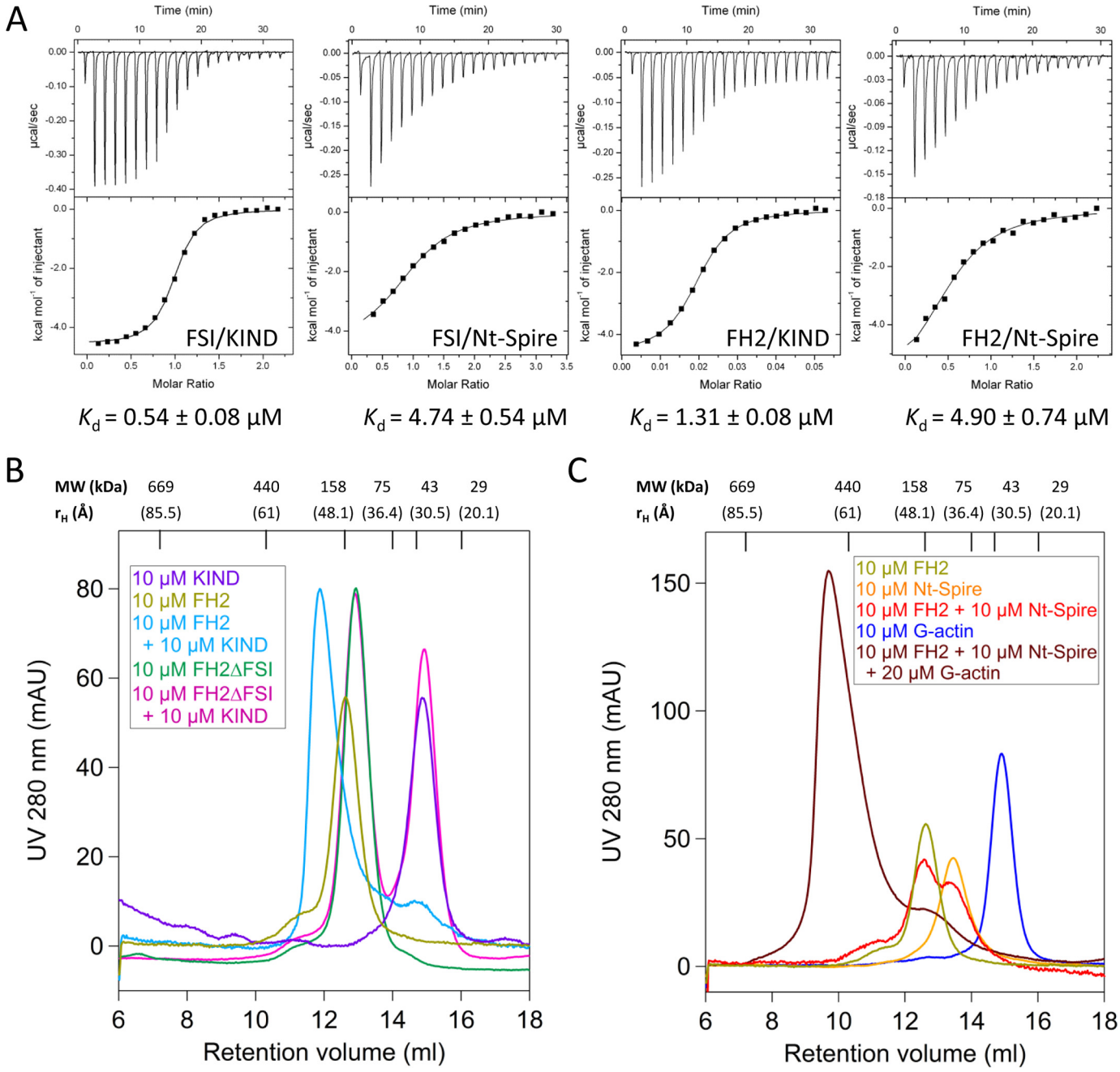

FIGURE 5. **Interaction between FSI of Fmn2 and the KIND domain of Nt-Spire is affected by the WH2 domains of Nt-Spire.** *A,* ITC measurements of FSI or FH2 binding to Spire constructs. The thermodynamic parameters of the interactions are listed in Table 2. *B* and *C,* analysis of FH2 complexes with Spire constructs by size exclusion chromatography. Gel filtration runs were performed in 150 mM NaCl with the indicated protein load. The calibration and Stokes radii are indicated. Consistent with ITC measurements (*A*), a tight 1:1 complex of FH2 and KIND co-eluted from the column, but no complex was formed between FH2ΔFSI and KIND (*B*). No complex was formed either between FH2 and Nt-Spire (*C*); however, when G-actin was present in the load together with FH2 and Nt-Spire, a stable ternary complex comprising FH2, Nt-Spire, and actin was eluted (*C*). *mAU*, milli-arbitrary unit.

TABLE 2

Thermodynamic parameters of formin 2 (Fmn2) and Spire interactions determined by isothermal titration calorimetry

All measurements were performed in 20 mM Tris/HCl, pH 7.5, 150 mM NaCl, 0.8 mM DTT at 25 °C.

Titration scheme[a]	K_a 10^5	K_d	ΔH	$T\cdot\Delta S$	ΔG	N
	M^{-1}	nM	kcal/mol	kcal/mol	kcal/mol	
FSI to KIND	12.1 ± 1.14	540 ± 77.6	−4.567 ± 0.042	3.727	−8.294	0.961 ± 0.006
FSI to Nt-Spire	2.11 ± 0.24	4740 ± 539	−4.496 ± 0.197	2.767	−7.263	0.973 ± 0.030
FH2 to KIND	7.66 ± 0.47	1305 ± 79	−4.656 ± 0.049	3.369	−8.025	0.821 ± 0.006
FH2 to Nt-Spire	2.04 ± 0.31	4901 ± 744	−6.456 ± 0.482	0.787	−7.243	0.554 ± 0.031

[a] Construct information is as follows: FSI peptide (Fmn2, amino acids 1549–1578), FH2 (Fmn2, amino acids 1139–1578), KIND (Spire1, amino acids 35–257), and Nt-Spire (Spire1, amino acids 1–443).

binding of FSI to the KIND domain of Nt-Spire indicates that the WH2 domains of Spire, by being bound to actin terminal subunits at barbed ends, no longer interfere with the binding of KIND to FSI in Fmn2. In contrast, the WH2 domains of Nt-Spire in solution are unliganded because G-actin is in complex with profilin. Therefore, free Nt-Spire shows reduced interaction with free Fmn2. The contact between the two proteins is thus specifically made at barbed ends.

FSI Interacts with G-actin at Low Ionic Strength and with F-actin at Barbed Ends as a Weak Capper—The binding of the C-terminal tail of Cappuccino to G-actin has been reported recently (15). We confirm that the very similar FSI of Fmn2 also binds with nanomolar affinity to G-actin in a 1:1 complex at low ionic strength. Binding was analyzed by monitoring either the change in fluorescence intensity of AEDANS-G-actin upon binding to FSI (Fig. 6*A*) or the increase in fluorescence anisotropy of AEDANS-labeled FSI (Cys-1695-labeled, see "Experimental Procedures") upon binding to unlabeled G-actin in G buffer (Fig. 6*B*). In both setups, formation of a 1:1 FSI·actin complex (K_d = 0.12 ± 0.01 and 0.11 ± 0.02 μM, respectively) was observed. The binding of FSI caused a 22% increase in AEDANS-actin fluorescence, consistent with establishing a more hydrophobic environment of the probe covalently attached to cysteine 374. In contrast, binding of WH2 domains or thymosin β4 generally quenches the fluorescence of AEDANS-actin, by making the environment of AEDANS more polar (30, 31). FSI bound G-actin in competition with thymosin β4 but did not compete with profilin, indicating that a ternary complex of actin with profilin and FSI formed in which the affinity of FSI (and of profilin as well) for G-actin is decreased by only 2–3-fold (Fig. 6*C*). Finally binding of FSI was highly sensitive to ionic strength. The affinity of FSI for G-actin decreased 60-fold at 50 mM KCl (Fig. 6*B*). No binding to G-actin could be detected at physiological ionic strength, in a micromolar range of concentration.

Because of its high content in basic residues, FSI bundles filaments in an ionic strength-sensitive manner, presumably by neutralizing the negatively charged N terminus of actin that is exposed at the surface of the filament. Bundling of F-actin by FSI was monitored by light scattering measurements at various ionic strengths (Fig. 6*D*) and microscopy assays (Fig. 6*E*). Bundling became undetectable above 75 mM KCl even at high concentrations of FSI (>10 μM). The bundling activities of FSI, Fmn2, and Fmn2ΔFSI in the concentration range of 0 to 2 μM were compared and are shown in Fig. 6*F*. The Fmn2 construct bundles filaments like FSI at 2 μM. No bundling by Fmn2ΔFSI was detected (Fig. 6*F*). Thus, bundling appears dependent on the presence of the FSI. Similar effects of the C-terminal extension of FMNL3 have been reported (34).

In spontaneous assembly assays using the fluorescence of pyrenyl-actin to monitor filament growth, FSI nucleated actin filaments at low ionic strength in the presence of profilin (1 mM $MgCl_2$, no KCl; Fig. 7*A*). The homolog tail region of Capu has likewise been reported to exhibit nucleation activity in a dimeric context yet in the absence of profilin (15). The nucleation activity of Fmn2's FSI motif was sensitive to ionic strength and already greatly reduced at 50 mM KCl (Fig. 7*B*). It is likely that the basic nature of FSI is also involved in its nucleation activity. The negative repulsive charges of actin monomers are reduced upon binding to FSI, which energetically facilitates the formation of pre-nuclei actin dimers.

In seeded barbed end growth assays at 50 mM KCl, FSI slowed down growth from profilin·actin. The level of F-actin assembly reached a lower pseudo-plateau, consistent with FSI capping barbed ends, causing sequestration of G-actin by profilin (Fig. 7*C*). However, the fluorescence pseudo-plateau continued to slowly increase. The capping activity was weaker at physiological ionic strength (100 mM KCl, Fig. 7*D*). After overnight incubation, the amount of F-actin at steady state in the presence of profilin appeared higher than the pseudo-plateau reached after 2 h in 50 mM KCl, and it was clearly unaltered at 100 mM KCl (Fig. 7*D*, *inset*). Consistently, only transient sequestration of G-actin by profilin was monitored upon varying profilin at a constant FSI concentration, and a pseudo-plateau of F-actin was reached (Fig. 7*E*), although higher amounts of F-actin were measured at steady state (Fig. 7*F*). We conclude that the FSI peptide is a weak, leaky barbed end capper, meaning that its affinity for barbed ends is too low to maintain the pointed end critical concentration. FSI also inhibited disassembly from the barbed end (Fig. 8*A*) but not from the pointed end (Fig. 8*B*), testifying that FSI slows down disassembly by binding barbed ends and not by stabilizing filaments by side binding. Finally all data presented in Fig. 7 are identical when KCl was replaced by NaCl (data not shown).

The weak capping activity of FSI and its effect on the fluorescence of the AEDANS probe bound to cysteine 374 of actin implies that it binds the barbed face of a terminal actin subunit at filament barbed ends. Bundling cannot be considered as functionally relevant when FSI is included in the FH2 domain of Fmn2 and committed to interact with actin at barbed ends.

Role of the Acidic Patch (Glu-1546, Glu-1548, and Glu-1549) N-terminal to the FSI Motif in the αT-helix of Fmn2—The fact that the effects of FSI on Fmn2 processivity are dependent on electrostatic interactions prompted us to examine the charged amino acids in the vicinity of FSI in the FH2 sequence. The αT-helix of FH2 is mainly positively charged except for three clustered glutamates (Glu-1546, Glu-1548, and Glu-1549). This acidic patch appears conserved among FH2 domains of formins (Fig. 1*A*). A triple point mutation of the three glutamates to alanines generated the Fmn2EA mutant and with additional deletion of the FSI motif the Fmn2EAΔFSI derivative (Fig. 1*A*).

Functional characterization of Fmn2EA showed that the mutation only slightly affected the ability of Fmn2 to nucleate filament assembly, to be stimulated by Nt-Spire, and to drive processive assembly at the same rate (51.6 subunits/s) as Fmn2 (Fig. 9, *A* and *B*). In contrast, although KIND inhibited nucleation by Fmn2 and Fmn2EA with practically identical efficiency (data not shown), the complex of KIND with Fmn2EA failed to inhibit barbed end elongation demonstrated for Fmn2·KIND (Fig. 9*C*). It also barely inhibited depolymerization (data not shown). Consistently, Fmn2EAΔFSI displayed a weaker inhibition of nucleation than Fmn2ΔFSI (data not shown) and failed to cap filament barbed ends significantly, at 50 and 100 mM NaCl both in seeded barbed end growth assays (Fig. 9*D*), and in measurements of F-actin at steady state (Fig. 1*F*). The weak capping activity of Fmn2EAΔFSI at 50 mM NaCl was analyzed

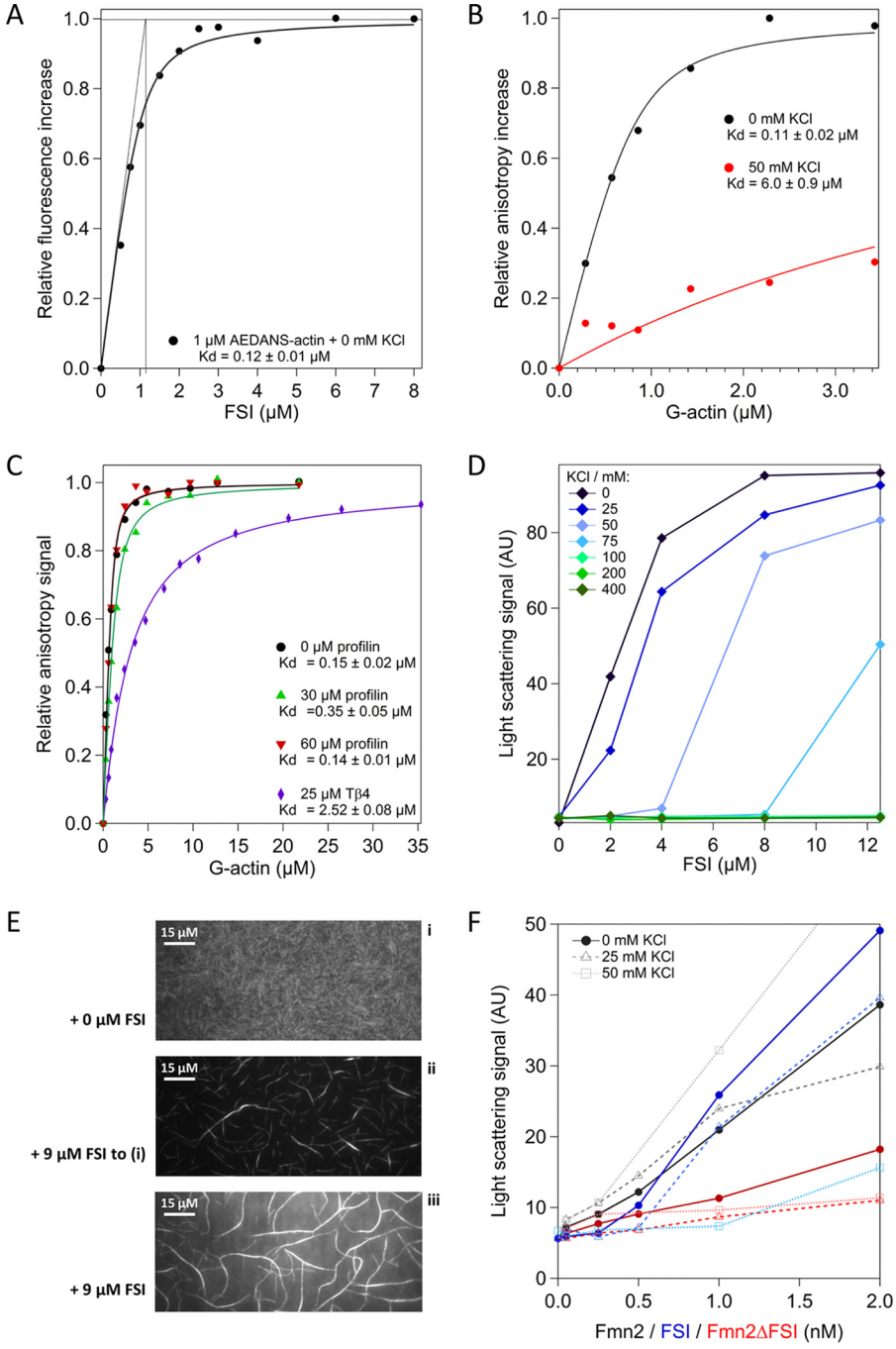

FIGURE 6. **FSI tail of Fmn2 binds G-actin and bundles F-actin.** *A,* increase in fluorescence of AEDANS-labeled G-actin (1 μM) upon binding to FSI. The fluorescence intensity of G-actin is normalized to 1. Symbols are data; line is calculated best fit binding curve using $f(B_0) = (B_0 + A_0 + K_d - ((B_0 + A_0 + K_d)^2 - 4 \cdot A_0 \cdot B_0)^{1/2})/(2 \cdot A_0)$ (see under "Experimental Procedures"). The derived K_d value is indicated. *B,* fluorescence anisotropy measurement of the binding of AEDANS-FSI (0.8 μM) to CaATP-G-actin, in low ionic strength G buffer (*black,* $K_d = 0.11 \pm 0.02$ μM) and at 50 mM NaCl (*red*, $K_d = 6.0 \pm 0.9$ μM). *C,* thymosin β4, but not profilin, inhibits binding of FSI to G-actin. AEDANS-labeled FSI (0.8 μM) in G buffer was titrated by G-actin in the absence (*black*, $K_d = 0.15 \pm 0.02$ μM) and presence of 25 μM thymosin β4 (*blue,* apparent $K_d = 2.52 \pm 0.08$ μM), 30 μM (*green*), or 60 μM (*red*) profilin. *D,* light scattering monitoring of filament bundling by FSI at 310 nm. Actin was assembled at 6 μM in the presence of the indicated concentrations of FSI and KCl. The intensity of scattered light reached a maximum in less than 1 h. The maximum intensity is plotted *versus* FSI concentration. Note that no bundling was detected at 100 mM KCl and above. *E,* fluorescence microscopy evidence for bundling of filaments by FSI. Time lapse images of actin filaments grown from 1 μM actin (10% Alexa-488-labeled) and 4 μM profilin in the absence (*panel i*) or presence (*panels ii* and *iii*) of 9 μM FSI are shown. *Panel ii*, 9 μM FSI was added to pre-grown filaments from *panel i*. For details see under "Experimental Procedures." *F,* compared bundling activities of FSI (*blue*), Fmn2ΔFSI (*red*), and Fmn2 (*black*) at 0 mM KCl (*deep color, circle*), 25 mM KCl (*medium tone, open triangle*), and 50 mM KCl (*light color, square*). *AU*, arbitrary units.

in single filament measurements (Fig. 9*E*). At 50 mM salt, Fmn2EAΔFSI capped barbed ends at a 2 orders of magnitude lower rate ($k_{on} = 0.06$ μM^{-1} s^{-1}; Fig. 9*E*) than Fmn2ΔFSI (Fig. 3*B* and Table 1), although they dissociate from barbed ends at identical rate (0.0035 s^{-1}). In conclusion, the acidic patch upstream from the FSI in the FH2 domain modulates the function of FSI in the association of Fmn2 to barbed ends and the control of processivity.

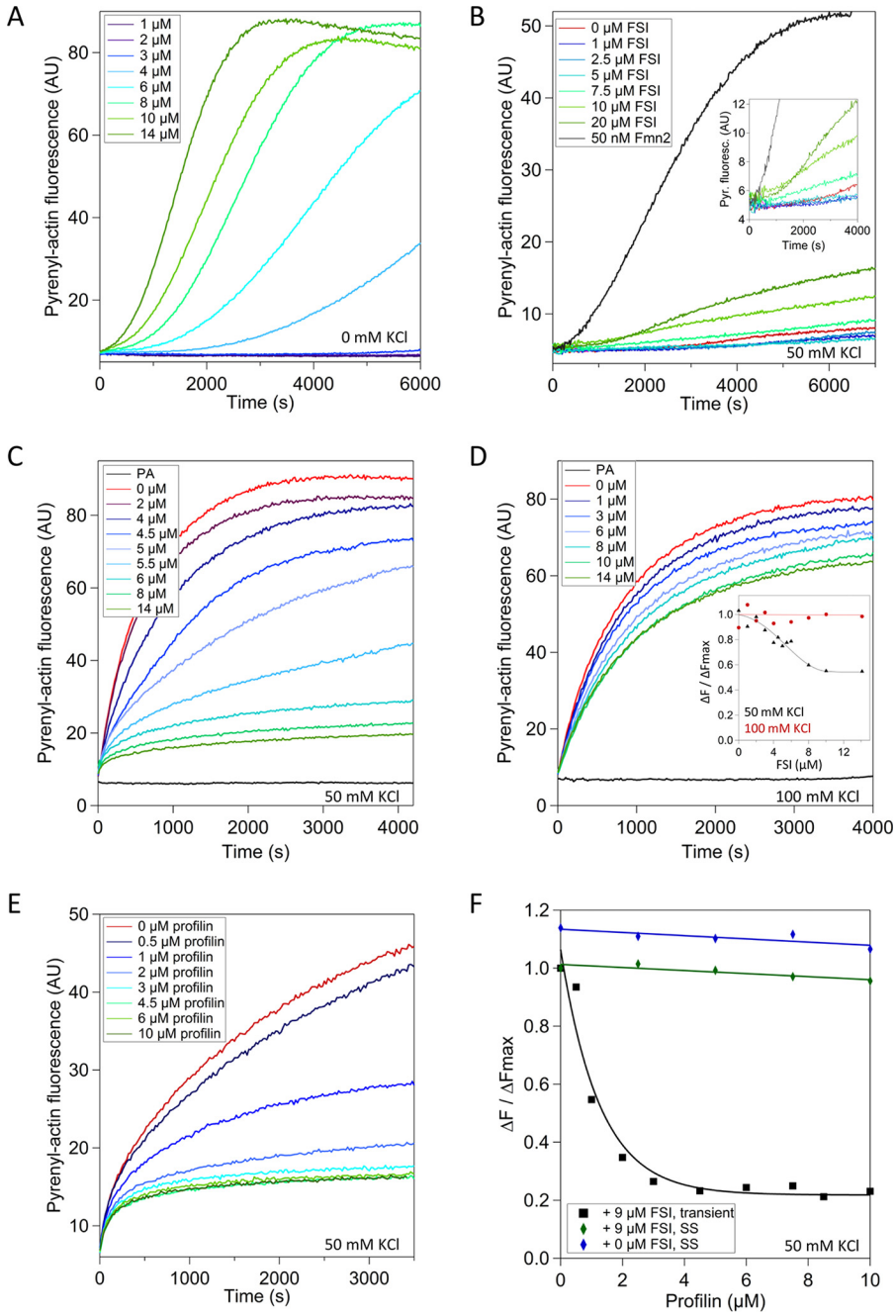

FIGURE 7. **FSI nucleates F-actin at low salt and slows down barbed end dynamics as a weak capper.** *A,* pyrenyl-actin fluorescence assay of spontaneous assembly of actin (4 μM) in the presence of 7.5 μM profilin and indicated amounts of FSI, at low ionic strength F buffer (1 mM $MgCl_2$ only, no KCl, 0.2 mM EGTA). *B,* same as in *A* except for the presence of 50 mM KCl. *C,* seeded barbed end growth of filaments in the presence of 0.42 nM spectrin-actin seeds, 2.5 μM actin (5% pyrenyl-labeled), 7.5 μM profilin, and indicated amounts of FSI at 50 mM KCl. *D,* same assay as in *C* except for the presence of 100 mM KCl. *Inset,* measured levels of pyrenyl-actin fluorescence at steady state after overnight incubation (*red dots*), in comparison with parallel samples at 50 mM KCl (*black triangles,* from *C*). *E,* seeded barbed end growth assays of actin filaments in the presence of 9 μM FSI show increased inhibition by profilin and evidence for a lower amount of F-actin at 4000 s. Experiments were performed with 0.42 nM spectrin-actin seeds, 2.5 μM actin (5% pyrenyl-labeled), 9 μM FSI, and indicated amounts of profilin in F buffer with 50 mM KCl. *F,* intensity of pyrenyl-actin fluorescence reached in *E* at 4000 s is plotted *versus* the concentration of profilin (*black squares*) together with the fluorescence intensity measured at steady state after overnight incubation (*green diamonds*). The fluorescence of control samples without FSI at steady state is in *blue diamonds*. *AU*, arbitrary units.

Discussion

The present results bring insight into the role of the C-terminal region of Fmn2 in its processive activity and into the molecular mechanism of synergy between Spire and Fmn2. In addition to its function in directing Fmn2 to Nt-Spire-bound barbed ends, the C-terminal extension (FSI) of the FH2 domain of Fmn2 plays an important role in assisting the processive walk of Fmn2. Although the FSI differs in sequence from other C-terminal extensions of the FH2 domains in various formins, either the DAD domain (32) or the WH2 domain of INF2 (33) and the WH2-like domain of FMNL3 (34), all these C-terminal extensions play similar roles in the regulation of formin processivity. In particular, the WH2-like C terminus of FMNL3 binds the barbed face of terminal F-actin subunits and inhibits

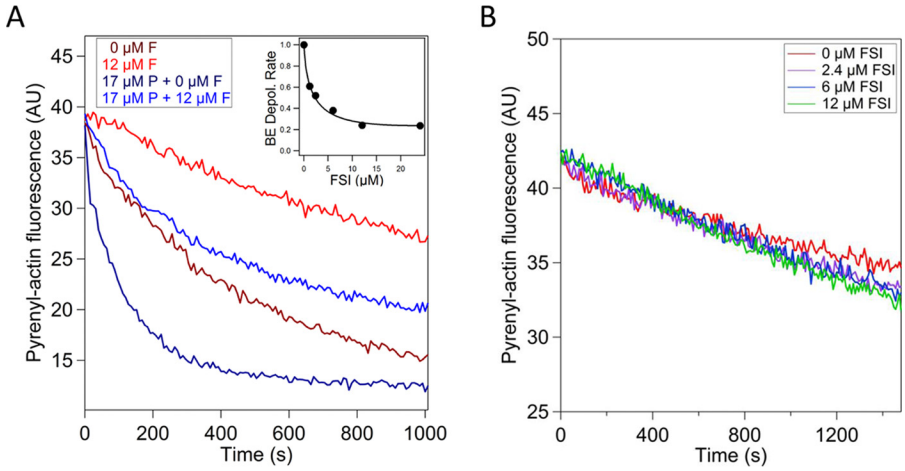

FIGURE 8. **FSI blocks barbed end disassembly but does not affect pointed ends.** *A,* dilution-induced depolymerization of filaments at barbed ends is slowed down by FSI. F-actin (5 μM, 5% pyrenyl-labeled) was diluted 16-fold in F buffer containing 50 mM KCl, with FSI (*F*) and profilin (*P*) as indicated. *Inset,* concentration dependence of the normalized rate of actin filament disassembly as a function of FSI concentration. *B,* FSI does not inhibit depolymerization from the pointed ends. Dilution-induced depolymerization of gelsolin-capped filaments (2.5 μM F-actin 5% pyrenyl-labeled, 8 nM gelsolin). Gelsolin-filaments were diluted 50-fold in F buffer (50 mM KCl) containing the indicated amounts of FSI. *AU*, arbitrary units.

barbed end growth like FSI. Similarly, the C-terminal tail of the Bud6 protein of budding yeast, comprising a WH2-like motif followed by a second α-helix, enhances the nucleation activity of the Bni1 formin (35). Therefore, a common basic mechanism may support the role of these different C-terminal regions of formins or of formin complexes with activators.

In direct line with our previous study, we investigated the role of the short C-terminal extension of the Fmn2 FH2 domain on our chimeric mDia1/FH1-Fmn2/FH2 construct that recapitulates all properties of Fmn2 FH1-FH2 (19). The similar activities of Fmn2ΔFSI and FH2ΔFSI reported here corroborate the view that the FH1 domain is not involved in the effects of FSI. Functional analyses of Fmn2ΔFSI on the one hand and of the isolated FSI on the other hand lead to consistent conclusions. Deletion of the FSI motif abolishes the nucleation activity of Fmn2, corroborating observations made by Vizcarra *et al.* (15) on C-terminally truncated Capu(CT-1031). More importantly, we find that removal of FSI converts Fmn2 into a barbed end capping protein. The capping activity, which is readily visible for Fmn2ΔFSI in bulk solution assays as well as in microfluidics assisted fluorescence microscopy, was not detected for CapuCT-1031 in TIRF assays on single filaments, for reasons that are not clear. Although the *Drosophila* and mammalian FH2 domains are very similar, it is possible that small differences in the sensitivity of Fmn2ΔFSI and CapuCT-1031 to ionic strength, due to a different C-terminal surface charge, have prevented the detection of the capping effect due to removal of the FH2 tail by Vizcarra *et al.* (15). The main effect of FSI removal consists in a very large increase in the association rate of Fmn2 to the filament barbed end, which contrasts with the remarkably slow association rate of the non-truncated protein (19). In contrast, the dissociation rate from barbed ends is not affected by FSI removal, and Fmn2 as well as Fmn2ΔFSI identically cap barbed ends in disassembly assays. This suggests that the influence of FSI on Fmn2 binding kinetics to the barbed ends differs between the elongation and the disassembly regime. Disassembly was monitored by dilution in a buffer that does not contain actin. The conformation of Fmn2 and Fmn2ΔFSI bound at barbed ends may thus differ depending on the ability of FH1-FH2 to interact with profilin-ATP-actin. It is also possible that the nature of the nucleotide bound at terminal subunits (ATP in a regime of filament assembly and ADP in a regime of disassembly) affects the strength of Fmn2 binding in an FSI-dependent manner. In this view, removal of FSI from Fmn2 would favor the closed, ADP-bound, capping state of the barbed end. These observations call for more detailed kinetic studies of association of Fmn2 and Fmn2ΔFSI with filament barbed ends.

The strength of barbed end capping depends on electrostatic contacts between Fmn2ΔFSI and terminal actin subunits. Capping is more leaky at 100 mM than at 50 mM NaCl. In addition, at 100 mM salt, Fmn2ΔFSI performs a few rare processive excursions at barbed ends, at the same rate as the unmodified Fmn2. Vizcarra *et al.* (15) found that removal of the tail in Capu enhances the rate of dissociation and thus decreases the dwell time of formin at barbed ends, without affecting the rate of processive assembly. The reason for the differences between Capu and Fmn2 regarding the role of the FSI is not clear.

The fact that the FSI almost abolishes the association of Fmn2 to filament barbed ends suggests that it may interfere with structural elements of FH2 involved in actin binding, while keeping its binding to KIND exposed. Glutamate to alanine mutations of the upstream acidic patch in the αT-helix in the Fmn2EA mutant do not modify the function of Fmn2 nor its interaction with KIND, but either removal of FSI from or association of KIND with Fmn2EA fails to induce barbed end capping. This piece of the data clearly indicates that the electrostatic environment of the FSI region in FH2 modulates its function in processivity. To integrate our results in the processive cycle of open to closed configurations of FH2 bound to growing barbed ends (13), we propose that FSI assists the transition toward the open configuration as follows. Because the isolated FSI motif binds actin at its barbed face in competition with thymosin β4 and slows down both filament barbed end growth and disassembly, it may compete with the knob region of the FH2 domain in the Fmn2 context, thus facilitating the transition to the open state.

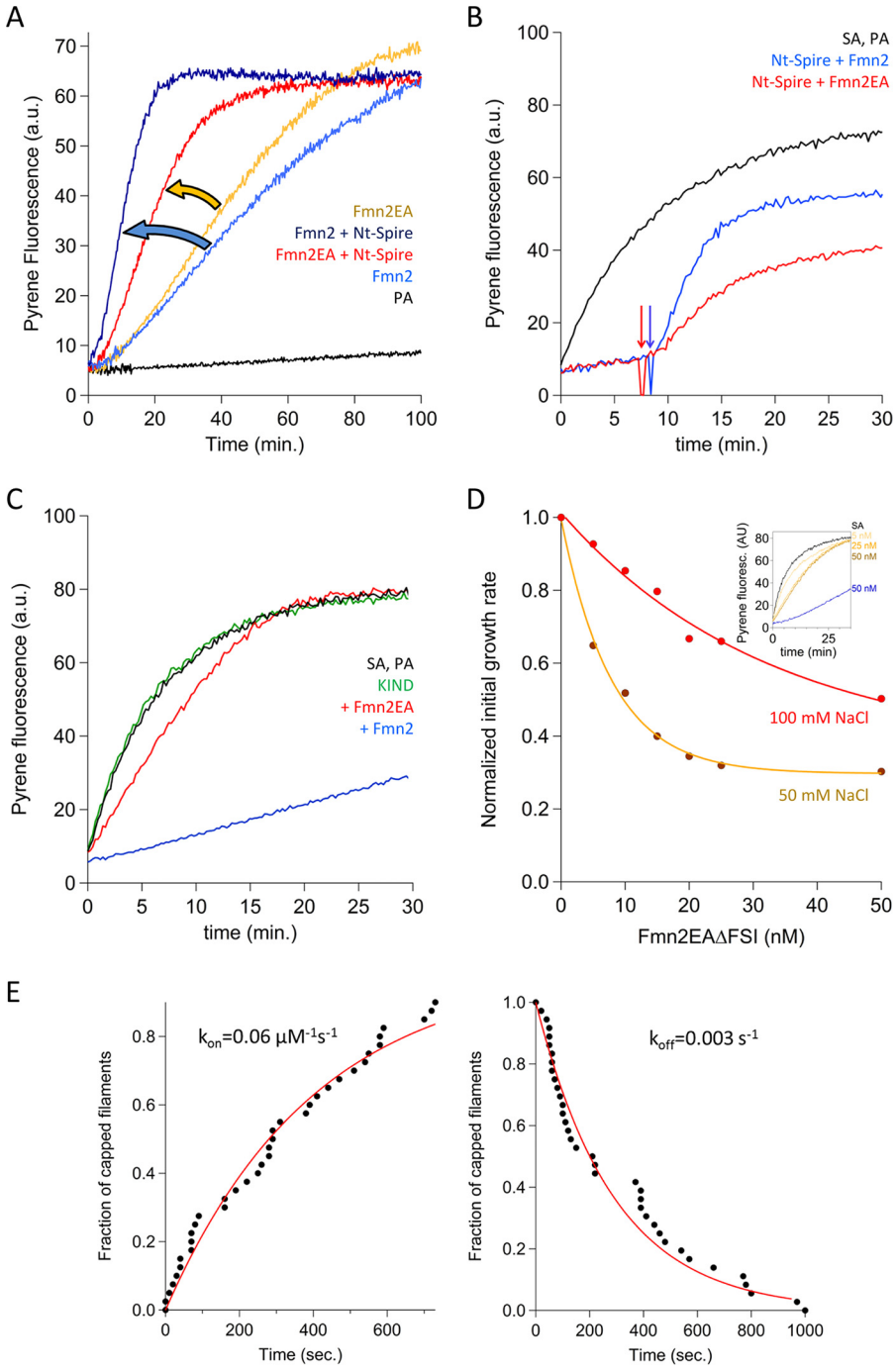

FIGURE 9. **Functional characterization of Fmn2EA and Fmn2EAΔFSI mutants.** *A,* nucleation activity of Fmn2 and its stimulation by Spire are maintained in the Fmn2EA mutant. Spontaneous assembly of pyrenyl-labeled actin (2.5 μM, 5%) in the presence of profilin (6 μM) and either Fmn2 or Fmn2EA (25 nM), with or without Nt-Spire (25 nM). *B,* Fmn2EA binds to Nt-Spire-capped filaments and induces barbed end growth. Spectrin·actin seeded (0.3 nM) barbed end elongation from profilin·actin (2.5 μM 5% pyrenyl-labeled actin, 6 μM profilin, *black curve*) in 50 mM NaCl was arrested by 100 nM Nt-Spire and restored by addition (*arrows*) of either 100 nM Fmn2 (*blue*) or Fmn2EA (*red*). *C,* complex of Fmn2EA with KIND fails to cap barbed ends. Spectrin·actin seeded (0.3 nM) barbed end growth at 50 mM NaCl is monitored in the presence of 2.5 μM G-actin (5% pyrenyl-labeled) and 6 μM profilin (*black curve*), and with the indicated additions of KIND alone (200 nM, *green curve*), and of KIND with either 100 nM Fmn2 (*blue curve*) or Fmn2EA (*red curve*). *D,* Fmn2EAΔFSI caps barbed ends very weakly. Rates of barbed end growth were monitored as in *C*, with addition of increasing amounts of Fmn2EAΔFSI, in the presence of 50 mM NaCl (*orange symbols*) or 100 mM NaCl (*red symbols*). *Inset* shows raw data of seeded barbed end growth at 50 mM NaCl (*black curve*) with increasing amounts of Fmn2EAΔFSI (*yellow curves*). A control curve (50 nM Fmn2EAΔFSI, without seeds) is shown in *blue*. *E,* single filament kinetic analysis of barbed end association of Fmn2EAΔFSI to barbed ends (*left, n* = 41) and of its dissociation from barbed ends (*right, n* = 35). *a.u.*, arbitrary units.

The isolated KIND domain of Spire binds Fmn2 in a complex that functionally mimics deletion of FSI. We conclude first that the FSI motif in Fmn2 is exposed to KIND, and second that the interaction between FSI and KIND in the Fmn2·KIND complex is equivalent to removal of FSI from Fmn2 without affecting the rest of the Fmn2 moiety. The contacts between FSI and KIND abolish the function of FSI in processivity; thus, the Fmn2·KIND complex behaves as a barbed end capper. The

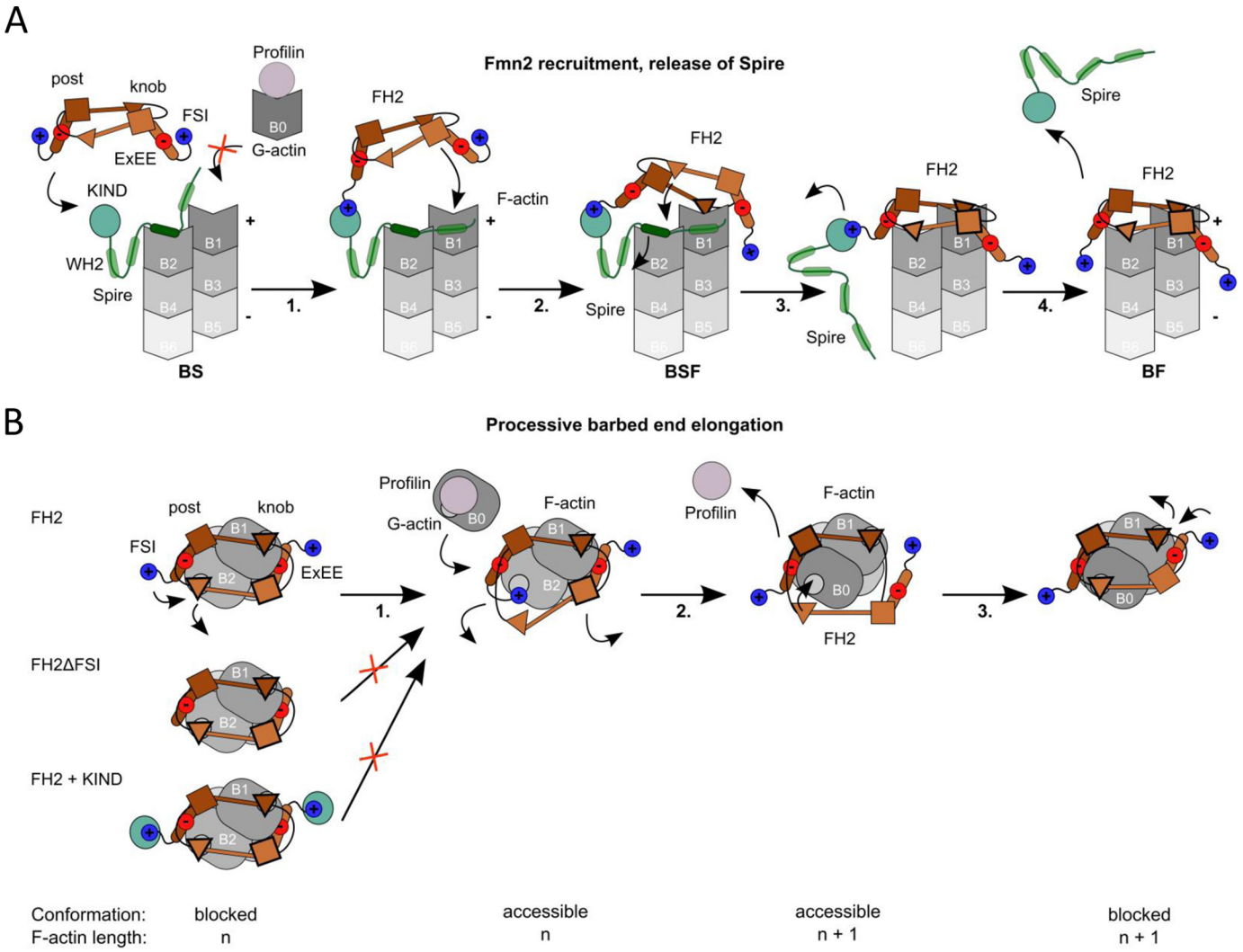

FIGURE 10. **Model for FSI function in Spire-mediated activation and in processive barbed end elongation by Fmn2.** The model is based on the presented results and published structural and molecular dynamic studies. For simplicity, only the FH2 domain (*brown*) with the adjacent FSI motif (*blue circle, plus*) of Fmn2 and the KIND domain (*blue-green*) followed by the four WH2 domains (*green*) of Nt-Spire are shown. The FH2 dimer is presented according to Otomo *et al.* (13) and interacts with its knob (*triangle*) and its post (*square*) subdomains with the terminal actin protomers B1 and B2 at the barbed end. Barbed end-bound subdomains are highlighted with *thick contours*. According to molecular dynamics studies (38) and structural modeling, the acidic motif in the αT-helix may interact with a basic surface formed by subdomain 1 of subunit B3 (αT of leading $FH2_1$ hemidimer, *dark brown*) and additionally the D-loop of B1 (αT of successive $FH2_2$ hemidimer, *light brown*). The FH2-knob, Spire-WH2, and FSI of hemidimer $FH2_1$ show overlapping binding sites at the barbed face of the terminal actin subunits. Abbreviations used are as follows: BS or BF, Spire- or Fmn2-bound barbed end; BSF, barbed end·Spire·Fmn2 complex; B1–6, terminal actin protomers of barbed end; B0, incoming G-actin; E*X*EE (*red circle, minus*), acidic cluster in αT-helix; post, knob, αT, structural elements of FH2 domain. *A,* side view of barbed end interactions. Fmn2 association with Nt-Spire via FSI-KIND contact is *step 1*; association of FH2 to barbed end (*step 2*) is followed by displacement of WH2 from B2 (*step 3*), and loss of affinity of Nt-Spire for FSI and release of Nt-Spire is *step 4*. For simplicity, the potential E*X*EE and FSI interactions with the barbed end are not depicted (see *B*). The representation of Spire at the barbed end is speculative because the exact binding mode is not known. One WH2 domain is tentatively bound. See under "Discussion" for details. *B,* proposed contribution of FSI to processivity of Fmn2. *Top view* on F-actin barbed end in the BF state is from *A* (*right*). The E*X*EE motif in FH2 interacts with the side of the barbed end. The FSI in the FH2 construct competes with the knob on B2, facilitating association of B0. This competition cannot take place upon binding of either FH2ΔFSI or FH2-KIND, which remains bound to B1 and B2 in the blocked state. The knob of the other FH2 hemidimer binds to B0, although the FSI of the other hemidimer can compete with the knob bound to B1. The sequence shown represents a cycle of FSI-assisted processive assembly. See under "Discussion" for details.

strong bonds made by the FH2 knob with the terminal subunits cannot be relieved by FSI in presence of KIND, and hence the closed state is maintained.

These conclusions are integrated in the following tentative model for FSI function in Fmn2 processivity and its activation by Nt-Spire (Fig. 10). How Spire activates Fmn2 is described in Fig. 10*A*. First, Nt-Spire caps the filament barbed end by association of at least one of its four WH2 domains to the barbed face of the B2 F-actin subunit. The KIND domain of barbed end-bound Nt-Spire is exposed to FSI, because the FSI·Nt-Spire complex caps barbed ends (19). Consistent with ITC measurements and size exclusion chromatography data, the KIND domain of Nt-Spire can interact with the FSI of Fmn2, because the WH2 domain moiety of Nt-Spire, which by itself weakens the KIND-FSI interaction, is bound to terminal F-actin. Thus, Fmn2 is recruited to barbed end-bound Nt-Spire (Fig. 10*A*, *step 1*). The knob region of one of the hemidimers of Fmn2 then associates with subunit B1 (Fig. 10*A*, *step 2*). We hypothesize that this association weakens the binding of the WH2 to actin and promotes its dissociation from actin B2 and its replacement

by the knob of the second hemidimer of Fmn2 (Fig. 10*A*, *step 3*). Once in their unliganded state, the WH2 domains lower the affinity of KIND for FSI, which triggers the dissociation of Nt-Spire from barbed ends and leaves Fmn2 bound in a closed capping state (Fig. 10*A*, *step 4*). Note that when KIND instead of Nt-Spire is bound, this change in affinity cannot occur, and Fmn2·KIND remains bound in the capping state. The dissociation of Nt-Spire initiates the regulatory activity of FSI in the processive walk of Fmn2 at barbed ends, as described in Fig. 10*B*. In this proposed scheme, FSI facilitates dissociation of the knob region of FH2 from B2, thus allowing association of a new profilin·actin subunit B0 (the FH1 bound to profilin is not represented for simplicity) (Fig. 10*B*, *step 1*). Following release of profilin, the knob region binds to the barbed face of B0 (Fig. 10*B*, *step 2*), and the FSI moiety of the other FH2 hemidimer displaces the knob bound to B1, starting a new cycle of assembly (Fig. 10*B*, *step 3*).

A few points remain speculative in this model, because the structural details of the binding of the WH2 domains of Spire to the filament barbed end are not known. The binding of one Spire to the penultimate actin subunit suffices to cap barbed ends and agrees with Ito *et al.* (36). In contrast, each of the FH2 hemidimers is able to bind a KIND domain (Fig. 4, *A* and *B,* and Table 2) (16). In this scheme, recruitment of Fmn2 by barbed end-bound Spire via association of KIND to one FSI of the Fmn2 dimer allows the FSI of the other arm to interact with the terminal actin subunit at the barbed end. The processive walk of the FH2 domain actually implies a non-symmetric actin-binding mode of the two FH2 hemidimers. In a subsequent step, displacement of the WH2 domain of Spire by the former FH2 arm would lower the affinity of KIND for its bound FSI (Table 2), promoting Spire dissociation from Fmn2. More extensive experimentation will have to be performed to explore these possibilities.

As outlined above, other formins are activated by actin-binding protein domains that act either externally (like Bud6, which activates Bni1 and also binds actin in a WH2-like fashion (35, 37) or internally (like the C-terminal WH2 domain of INF2 or FMNL3 (30, 31)). The model we present here for the role of FSI in the processive function of Fmn2 may thus have general significance regarding the regulation of other formins.

Author Contributions—M. F. C. designed the research; P. M. and S. K. conducted the research; C. C. provided technical help; M. F. C. wrote the paper with P. M. and S. K.

Acknowledgments—This work benefited from the IMAGIF platform facilities at the Centre de Recherche de Gif-sur-Yvette (FRC3115, CNRS, France) for microcalorimetry work. We thank Bérengère Guichard for technical assistance.

References

1. Carlier, M. F., Pernier, J., Montaville, P., Shekhar, S., Kühn, S., and Cytoskeleton Dynamics and Motility Group (2015) Control of polarized assembly of actin filaments in cell motility. *Cell. Mol. Life Sci.* **72,** 3051–3067
2. Goode, B. L., and Eck, M. J. (2007) Mechanism and function of formins in the control of actin assembly. *Annu. Rev. Biochem.* **76,** 593–627
3. Pruyne, D., Evangelista, M., Yang, C., Bi, E., Zigmond, S., Bretscher, A., and Boone, C. (2002) Role of formins in actin assembly: nucleation and barbed-end association. *Science* **297,** 612–615
4. Carlier, M. F., Pernier, J., and Avvaru, B. S. (2013) Control of actin filament dynamics at barbed ends by WH2 domains: from capping to permissive and processive assembly. *Cytoskeleton* **70,** 540–549
5. Azoury, J., Lee, K. W., Georget, V., Rassinier, P., Leader, B., and Verlhac, M. H. (2008) Spindle positioning in mouse oocytes relies on a dynamic meshwork of actin filaments. *Curr. Biol.* **18,** 1514–1519
6. Dahlgaard, K., Raposo, A. A., Niccoli, T., and St Johnston, D. (2007) Capu and Spire assemble a cytoplasmic actin mesh that maintains microtubule organization in the *Drosophila* oocyte. *Dev. Cell* **13,** 539–553
7. Emmons, S., Phan, H., Calley, J., Chen, W., James, B., and Manseau, L. (1995) Cappuccino, a *Drosophila* maternal effect gene required for polarity of the egg and embryo, is related to the vertebrate limb deformity locus. *Genes Dev.* **9,** 2482–2494
8. Leader, B., Lim, H., Carabatsos, M. J., Harrington, A., Ecsedy, J., Pellman, D., Maas, R., and Leder, P. (2002) Formin-2, polyploidy, hypofertility and positioning of the meiotic spindle in mouse oocytes. *Nat. Cell Biol.* **4,** 921–928
9. Manseau, L., Calley, J., and Phan, H. (1996) Profilin is required for posterior patterning of the *Drosophila* oocyte. *Development* **122,** 2109–2116
10. Pfender, S., Kuznetsov, V., Pleiser, S., Kerkhoff, E., and Schuh, M. (2011) Spire-type actin nucleators cooperate with Formin-2 to drive asymmetric oocyte division. *Curr. Biol.* **21,** 955–960
11. Quinlan, M. E., Hilgert, S., Bedrossian, A., Mullins, R. D., and Kerkhoff, E. (2007) Regulatory interactions between two actin nucleators, *Spire* and *Cappuccino. J. Cell Biol.* **179,** 117–128
12. Wellington, A., Emmons, S., James, B., Calley, J., Grover, M., Tolias, P., and Manseau, L. (1999) Spire contains actin binding domains and is related to ascidian posterior end mark-5. *Development* **126,** 5267–5274
13. Otomo, T., Tomchick, D. R., Otomo, C., Panchal, S. C., Machius, M., and Rosen, M. K. (2005) Structural basis of actin filament nucleation and processive capping by a formin homology 2 domain. *Nature* **433,** 488–494
14. Xu, Y., Moseley, J. B., Sagot, I., Poy, F., Pellman, D., Goode, B. L., and Eck, M. J. (2004) Crystal structures of a formin homology-2 domain reveal a tethered dimer architecture. *Cell* **116,** 711–723
15. Vizcarra, C. L., Bor, B., and Quinlan, M. E. (2014) The role of formin tails in actin nucleation, processive elongation, and filament bundling. *J. Biol. Chem.* **289,** 30602–30613
16. Vizcarra, C. L., Kreutz, B., Rodal, A. A., Toms, A. V., Lu, J., Zheng, W., Quinlan, M. E., and Eck, M. J. (2011) Structure and function of the interacting domains of Spire and Fmn-family formins. *Proc. Natl. Acad. Sci. U.S.A.* **108,** 11884–11889
17. Zeth, K., Pechlivanis, M., Samol, A., Pleiser, S., Vonrhein, C., and Kerkhoff, E. (2011) Molecular basis of actin nucleation factor cooperativity: crystal structure of the Spir-1 kinase non-catalytic C-lobe domain (KIND)*formin-2 formin SPIR interaction motif (FSI) complex. *J. Biol. Chem.* **286,** 30732–30739
18. Bosch, M., Le, K. H., Bugyi, B., Correia, J. J., Renault, L., and Carlier, M. F. (2007) Analysis of the function of Spire in actin assembly and its synergy with formin and profilin. *Mol. Cell* **28,** 555–568
19. Montaville, P., Jégou, A., Pernier, J., Compper, C., Guichard, B., Mogessie, B., Schuh, M., Romet-Lemonne, G., and Carlier, M. F. (2014) Spire and Formin 2 synergize and antagonize in regulating actin assembly in meiosis by a ping-pong mechanism. *PLoS Biol.* **12,** e1001795
20. Almonacid, M., Ahmed, W. W., Bussonnier, M., Mailly, P., Betz, T., Voituriez, R., Gov, N. S., and Verlhac, M. H. (2015) Active diffusion positions the nucleus in mouse oocytes. *Nat. Cell Biol.* **17,** 470–479
21. Holubcová, Z., Howard, G., and Schuh, M. (2013) Vesicles modulate an actin network for asymmetric spindle positioning. *Nat. Cell Biol.* **15,** 937–947
22. Pernier, J., Orban, J., Avvaru, B. S., Jégou, A., Romet-Lemonne, G., Guichard, B., and Carlier, M. F. (2013) Dimeric WH2 domains in *Vibrio* VopF promote actin filament barbed-end uncapping and assisted elongation. *Nat. Struct. Mol. Biol.* **20,** 1069–1076
23. Shekhar, S., Kerleau, M., Kühn, S., Pernier, J., Romet-Lemonne, G., Jégou, A., and Carlier, M. F. (2015) Formin and capping protein together embrace the actin filament in a "ménage à trois". *Nat. Commun.* **6,** 8730
24. Shekhar, S., and Carlier, M. F. (2016) Kinetic studies provide key insights

into regulation of actin-based motility. *Mol. Biol. Cell* **27,** 1–6
25. Anthis, N. J., and Clore, G. M. (2013) Sequence-specific determination of protein and peptide concentrations by absorbance at 205 nm. *Protein Sci.* **22,** 851–858
26. Jégou, A., Niedermayer, T., Orbán, J., Didry, D., Lipowsky, R., Carlier, M. F., and Romet-Lemonne, G. (2011) Individual actin filaments in a microfluidic flow reveal the mechanism of ATP hydrolysis and give insight into the properties of profilin. *PLoS Biol.* **9,** e1001161
27. Carlier, M. F., Romet-Lemonne, G., and Jégou, A. (2014) Actin filament dynamics using microfluidics. *Methods Enzymol.* **540,** 3–17
28. Pechlivanis, M., Samol, A., and Kerkhoff, E. (2009) Identification of a short Spir interaction sequence at the C-terminal end of formin subgroup proteins. *J. Biol. Chem.* **284,** 25324–25333
29. Rosales-Nieves, A. E., Johndrow, J. E., Keller, L. C., Magie, C. R., Pinto-Santini, D. M., and Parkhurst, S. M. (2006) Coordination of microtubule and microfilament dynamics by Drosophila Rho1, *Spire* and *Cappuccino*. *Nat. Cell Biol.* **8,** 367–376
30. De La Cruz, E. M., Ostap, E. M., Brundage, R. A., Reddy, K. S., Sweeney, H. L., and Safer, D. (2000) Thymosin-β(4) changes the conformation and dynamics of actin monomers. *Biophys. J.* **78,** 2516–2527
31. Didry, D., Cantrelle, F. X., Husson, C., Roblin, P., Moorthy, A. M., Perez, J., Le Clainche, C., Hertzog, M., Guittet, E., Carlier, M. F., van Heijenoort, C., and Renault, L. (2012) How a single residue in individual β-thymosin/WH2 domains controls their functions in actin assembly. *EMBO J.* **31,** 1000–1013
32. Gould, C. J., Maiti, S., Michelot, A., Graziano, B. R., Blanchoin, L., and Goode, B. L. (2011) The formin DAD domain plays dual roles in autoinhibition and actin nucleation. *Curr. Biol.* **21,** 384–390
33. Chhabra, E. S., and Higgs, H. N. (2006) INF2 is a WASP homology 2 motif-containing formin that severs actin filaments and accelerates both polymerization and depolymerization. *J. Biol. Chem.* **281,** 26754–26767
34. Heimsath, E. G., Jr., and Higgs, H. N. (2012) The C terminus of formin FMNL3 accelerates actin polymerization and contains a WH2 domain-like sequence that binds both monomers and filament barbed ends. *J. Biol. Chem.* **287,** 3087–3098
35. Park, E., Graziano, B. R., Zheng, W., Garabedian, M., Goode, B. L., and Eck, M. J. (2015) Structure of a Bud6/Actin complex reveals a novel WH2-like actin monomer recruitment motif. *Structure* **23,** 1492–1499
36. Ito, T., Narita, A., Hirayama, T., Taki, M., Iyoshi, S., Yamamoto, Y., Maéda, Y., and Oda, T. (2011) Human spire interacts with the barbed end of the actin filament. *J. Mol. Biol.* **408,** 18–25
37. Tu, D., Graziano, B. R., Park, E., Zheng, W., Li, Y., Goode, B. L., and Eck, M. J. (2012) Structure of the formin-interaction domain of the actin nucleation-promoting factor Bud6. *Proc. Natl. Acad. Sci. U.S.A.* **109,** E3424–E3433
38. Baker, J. L., Courtemanche, N., Parton, D. L., McCullagh, M., Pollard, T. D., and Voth, G. A. (2015) Electrostatic interactions between the Bni1p Formin FH2 domain and actin influence actin filament nucleation. *Structure* **23,** 68–79